Sequentially Prepared Mo-V-Based SCR Catalyst for Simultaneous Hg(0) Oxidation and NO Reduction

Can Li [a], Vishnu Sriram [a], Zhouyang Liu [a], Dale Brewe [b], and Joo-Youp Lee [a,*]

[a] Chemical Engineering Program, Department of Chemical and Environmental Engineering, University of Cincinnati, Cincinnati, OH, 45221-0012, United States

[b] X-ray Science Division, Advanced Photon Source, Argonne National Laboratory, Argonne, IL 60439, United States

li2c2@mail.uc.edu, sriramvu@mail.uc.edu, liuzy@mail.uc.edu, brewe@aps.anl.gov, and joo.lee@uc.edu

[*] Corresponding author

Joo-Youp Lee

Chemical Engineering Program, Department of Chemical and Environmental Engineering, University of Cincinnati, Cincinnati, Ohio 45221-0012

Tel.: +1 513 566 0018; Fax: +1 413 566 0018.

E-mail: joo.lee@uc.edu (Joo-Youp Lee)

Abstract

Molybdenum (Mo)-vanadium (V)-based selective catalytic reduction (SCR) catalyst synthesized by the sequential impregnation of Mo and W followed by V was investigated for simultaneous elemental mercury (Hg(0)) oxidation and nitrogen oxide (NO) reduction in an existing SCR unit with respect to different TiO_2 phases, calcination temperatures, flue gas constituents, gas velocities, and reaction temperatures. Anatase phase TiO_2 and the calcination temperatures of 400 and 500 °C resulted in ~69% Hg(0) oxidation at 10 ppmv HCl and 350°C. The high calcination temperature of 700 °C resulted in TiO_2 phase transformation from anatase to rutile and agglomeration. The modified SCR catalyst prepared with the impregnation sequence of Mo and W followed by V using anatase TiO_2 and calcination temperature 500 °C showed ~99%

Hg(0) oxidation and 87% NO reduction conversions at an NH_3/NO molar ratio of 0.9 under 350 °C and 5,000 hr^{-1} space velocity in typical sub-bituminous and lignite coal simulated flue gases. The effects of these parameters and conditions were further investigated using various characterization techniques including BET, TEM, XRD, NH_3 TPD and XAFS.

Keywords: mercury oxidation, nitrogen oxide reduction, SCR catalyst, calcination temperature, and bimetallic catalyst.

1. Introduction

Coal-fired power plants are considered to be responsible for over 30% (>44 tonnes) mercury emissions from all kinds of anthropogenic sources every year in the United States.[1] There exist three different types of mercury in coal combustion exhaust gas including particulate-bound (Hg^p), oxidized (Hg^{2+}), and elemental (Hg^0).[2] Hg^p and Hg^{2+} can be easily separated using current conventional air pollution control systems, such as baghouse filter, electrostatic precipitator (ESP) and wet flue gas desulfurization (FGD).[3] Nevertheless, it is very challenging to separate Hg^0 species because it is highly volatile, very low in concentrations, and nearly insoluble in water. The Mercury and Air Toxics Standards (MATS) rule issued in 2012 the mercury emissions limits of 1.2 and 0.015 lb/TBtu (or 0.013 and 0.0002 lb/GWh) from existing and new coal-fired power plants, respectively. These regulation limits for existing and new coal-fired power plants are equivalent to ~90+ and ~99+% on a monthly rolling average basis, respectively. Therefore, the separation of Hg^0 is imperative to successfully comply with the current stringent regulations.

Existing mercury control technologies in the market include sorbent injection, fuel additives, selective catalytic reduction (SCR) optimization, and Hg^{2+} separation from wet FGD

system. Sorbent injection uses raw or chemically-modified activated carbon to collect Hg^0 and Hg^{2+}.[2-4] However, the cost is expensive.[5] Fuel additives including chlorine and bromine salts can be added to the power plant boiler to improve the Hg^0 oxidation capability.[6-8] However, it generally requires high halogen addition and can also cause a corrosion problem in the air preheater. Previous studies demonstrated that ~15% to 68% of Hg^0 vapor could be converted into Hg^{2+} form over SCR catalyst with HCl.[9-11] Currently, SCR units and wet FGD systems have been equipped in most coal-fired power plants. The number of SCR and wet FGD unit installations has increased due to the Cross State Air Pollution Rule (CSAPR) regulating NO_x and SO_2 emissions more stringently from fossil fuel-fired power plants in 27 states from 2012 in the United States. The Hg^0 to Hg^{2+} conversion over the SCR unit provides an opportunity to capture Hg^{2+} in a downstream wet FGD system to lower both mercury and NO_x emissions.

V_2O_5-WO_3 or V_2O_5-MoO_3 supported on TiO_2 are widely used as commercial SCR catalysts to reduce NO_x.[12-14] Previous studies on Hg^0 oxidation over V_2O_5-WO_3/TiO_2 reported limited Hg(0) oxidation capability under the condition of low HCl concentrations in sub-bituminous and lignite coal combustion flue gases.[9, 15, 16] To enhance the Hg^0 oxidation capability under low HCl concentrations, additional active metals such as Mn, Ce, Ru, Cu, and Fe have been attempted to optimize conventional SCR catalyst formulas.[17-24] However, all the above modified catalysts need additional equipment installations or changes in different operating temperatures. A few studies have been taken to explore Hg^0 oxidation over V_2O_5-MoO_3/TiO_2. A V_2O_5(5%)-MoO_3(5%)/TiO_2 catalyst synthesized using a sol-gel technique reported an up to 28% improvement in Hg^0 oxidation activity relative to an in-house V_2O_5(5%)/TiO_2 catalyst under 6%(v) O_2 and no HCl at 350 ºC.[25] A previous study using V_2O_5(5%)-MoO_3(5%)/TiO_2 reported that HCl and NO gases could positively affect Hg^0 oxidation activity while H_2O, SO_2, and NH_3 gases

showed an inhibitory effect.[26] The Hg(0) oxidation activity of the catalyst was higher than that of a fresh commercial SCR catalyst (V_2O_5(3.30%)-WO_3(2.27%)/TiO_2) regardless of NH_3 under actual flue gas conditions.[27]

Our previous study reported that the modified SCR catalyst prepared using the impregnation sequence of Mo and W followed by V exhibited ~69% Hg^0 oxidation activity at 10 ppmv HCl and 350 °C.[28] Meanwhile, the NO reduction activity was ~80% with respect to various metal loadings and impregnation sequences. The objective of this study is to examine the simultaneous Hg(0) oxidation and NO reduction in terms of different TiO_2 phases, calcination temperatures, flue gas constituents, gas velocities, and reaction temperatures over our Mo-V-based SCR catalyst. Different characterization techniques were employed to understand potential relationships between the different preparation conditions and catalytic activities. The study results can provide fundamental understanding and scientific insights for simultaneous mercury and NO_x emissions control in an existing SCR system.

2. Experimental

2.1. Catalyst synthesis

In this work, our Mo-V-based SCR catalyst was synthesized using incipient wetness impregnation with different TiO_2 supports and calcination temperatures.[29] It is the most widely cited method for supported metal oxide catalysts due to its simplicity and the ease of scalability.[30] Anatase TiO_2 (DT-51, from Cristal), mixed anatase/rutile TiO_2 (P25, from Sigma Aldrich) and rutile TiO_2 (STR-100W, from Sakai Chemical) were selected as the catalyst supports, respectively. Four different temperatures 400, 500, 600 and 700 °C were chosen as the calcination temperatures, respectively. The detailed synthesis procedures are shown in our previous publication.[28] The previous work demonstrated that the Mo-V-based SCR catalyst containing 0.5 wt.% V_2O_5, 7 wt.%

MoO_3 and 3 wt.% WO_3 with the impregnation sequence of Mo and W followed by V (i.e. $MoO_3(7)+WO_3(3)\rightarrow V_2O_5(0.5)/TiO_2$) had the best activity. Therefore, the same impregnation sequence and loading percentages of the metals have been used to prepare the modified SCR catalyst samples with different TiO_2 supports and calcination temperatures. The synthesized samples were designated as $MoO_3+WO_3\rightarrow V_2O_5/TiO_2$ A B, where A and B represented TiO_2 support and calcination temperature, respectively. Co-impregnation method was utilized to synthesize V-based conventional SCR catalyst with 0.5 wt.% V_2O_5 and 9 wt.% WO_3. This sample was denoted as V_2O_5+WO/TiO_2 DT-51 CT500. The pelletized catalyst was employed to conduct the catalytic activity test. The powdered catalyst was employed to carry out characterization analysis after grinding the pelletized catalyst.

2.2. Activity tests

The catalytic activity tests of the Mo-V-based SCR catalyst in terms of different TiO_2 supports and calcination temperatures were conducted in a fixed-bed reactor system as illustrated in Fig. 1 to evaluate their Hg^0 oxidation and NO reduction efficiencies. Hg^0 vapor was brought into the system by introducing 100 ml/min N_2 through a mercury permeation tube (VICI Metronics) located in a calibration gas generator oven (Dynacalibrator, VICI Metronics) and ~15 ppbv Hg(0) was used as a typical inlet concentration. All of the simulated flue gas constituents regulated through mass flow controllers were produced using gas cylinders and specified in Results and Discussions part. Water vapor was fed into the system through controlling the temperature of a water bubbler. The total flow rate of the simulated coal combustion flue gas was fixed at 1 L/min. Typically, a quartz reactor with a 16 mm inner diameter containing ~1.72 g of catalyst pellets was used to conduct the activity tests. The quartz reactor was placed in the center of a vertical oven equipped with a temperature controller. These tests were run under a gas hourly space velocity

(GHSV) of 40,000 hr^{-1} at 350 ºC to examine the catalytic activities of Hg(0) oxidation and NO reduction in terms of different TiO_2 supports and calcination temperatures.[16] When the effect of GHSV on the activities was investigated, a different catalyst amount was used to set the GHSV inside the reactor.

During all the catalytic activity tests, a cold vapor atomic absorption spectrophotometer (CVAAS, Model 400A, Buck Scientific Inc.) combined with Ontario Hydro Method was used to measure mercury concentrations at the inlet and outlet of the system. Two different impinger solutions: 1 M KCl and 4%(w/v) $KMnO_4$/10%(v/v) H_2SO_4 were employed to collect oxidized mercury and Hg^0 vapor, respectively. A Micro Emission Analyzer (Model 500, Enerac LLC) was employed to determine NO inlet and outlet concentrations. The activities of Hg^0 oxidation and NO reduction were calculated based on the inlet and outlet Hg(0) and NO concentrations as shown below.

$$\text{Hg(0) oxidation activity} = \frac{Hg^0_{in} - Hg^0_{out}}{Hg^0_{in}} \times 100\% \quad (1)$$

$$\text{NO reduction activity} = \frac{NO_{in} - NO_{out}}{NO_{in}} \times 100\% \quad (2)$$

2.3. Catalyst characterization

The Brunauer-Emmett-Teller (BET) surface area, pore volume and pore diameter of the Mo-V-based SCR catalysts were determined at 77 K by nitrogen adsorption using Micromeritics ASAP 2020. The catalyst morphology was analyzed using a FEI CM 20 transmission electron microscope (TEM). Isopropyl alcohol (IPA) was utilized to spread the ground catalyst to ensure that the catalyst powder was uniformly dispersed over a copper grid for TEM analysis.

The X-ray powder diffraction (XRD) analysis was conducted under an X'Pert Pro MPD X-ray diffractometer to measure the crystalline structure of the samples. The XRD diffractometer was equipped with Cu Kα radiation (λ=0.1543 nm). The ground catalyst powder was packed into a sample holder. The sample was scanned under a step time of 0.5 s in a range of 10° to 60° (2θ) with a step size of 0.02°.

Temperature-programmed desorption of NH_3 (NH_3-TPD) was conducted using AutoChem 2910 to determine the surface acidity of the sequentially modified SCR catalysts on different substrates. In a typical pretreatment process, ~100 mg catalyst was heated up to 500 °C with a ramp rate of 20 °C/min and held at this temperature for 1 hr under 20 ml/min He. Then, the sample was cooled down to room temperature and saturated with 4% NH_3 balanced with He at 30 ml/min for 30 min. At the end of the saturation procedure, pure He at 20 ml/min was used to flush over the sample for 30 min to remove weakly adsorbed NH_3. The thermal conductivity detector (TCD) signal was recorded while heating the sample up to 500 °C at a ramp rate of 15 °C /min in pure He for NH_3 desorption.

X-ray absorption near-edge structure (XANES) spectroscopy was conducted at Argonne National Laboratory (ANL, Chicago, IL). The data were taken on the 20-BM-B Beamline from the Advanced Photon Source (APS) with a Si (111) monochromator. The energy scale was calibrated at 5,465 eV by a V metal foil. Three different vanadium references containing V_2O_5, VO_2 and V_2O_3 were used to carry out the energy scale calibration. These references were finely pulverized using a mortar and evenly dispersed over Kapton tape. Then the folded tape was analyzed under transmission mode. Each sample was run at least three times to enhance the signal-to-noise ratio. Since the V concentration on synthesized SCR catalysts was low and the interference between V and Ti, a larger amount of sample was packed in a sample holder. To

analyze V in fresh modified SCR catalysts with different TiO_2 supports and calcination temperatures, these modified SCR samples were finely pulverized using a mortar and put into a Teflon holder. Then, the samples were tested in fluorescence mode. Each sample was run at least 8 scans to enhance the signal-to-noise ratio.

3. Results and Discussions

3.1. Effects of Preparation Parameters on Activities of Hg^0 oxidation and NO reduction

3.1.1. Effects of TiO_2 supports

TiO_2 is a widely used substrate resistant to metal sulfate formation in coal combustion flue gas containing SO_2. TiO_2-based catalysts are stable and has a resistance to sulfation in the SCR process.[31, 32] To explore the effects of different TiO_2 phases on simultaneous Hg^0 oxidation and NO reduction, the three different TiO_2 supports of anatase DT-51, 75 wt.% anatase/25 wt.% rutile P25, and rutile STR-100W were selected.

The activities of simultaneous Hg^0 oxidation and NO reduction over the Mo-V-based SCR catalysts with different TiO_2 phases were tested under a simulated lignite and sub-bituminous coal combustion flue gas condition and the activity results are exhibited in Fig. 2. For Hg(0) oxidation, among these three catalysts, anatase TiO_2 DT-51 supported Mo-V-based SCR catalyst exhibited the highest Hg^0 oxidation activity (~53% at 5 ppmv HCl and ~69% at 10 ppmv HCl) and NO reduction activity (~80%). When P25 was employed as a support, Hg^0 oxidation activity decreased to ~32% at 5 ppmv HCl and ~56% at 10 ppmv HCl, respectively. In the meantime, the NO reduction activity was kept the same at ~80% for both supports. When rutile STR-100W was used, the catalyst almost lost its Hg^0 oxidation ability and also showed the significantly decreased NO reduction activity of ~49%. This result shows that anatase phase TiO_2 should be used as a support for simultaneous Hg^0 and NO removal.

3.1.2. Effects of calcination temperatures

Calcination temperature is an important factor during SCR catalyst preparation. Because calcination temperature can affect phase transformation and active metal dispersion, it can influence SCR catalyst activity.[33-35] To probe the effect of calcination temperatures on simultaneous Hg^0 oxidation and NO reduction, four different calcination temperatures were selected. The activities of simultaneous Hg^0 oxidation and NO reduction over the Mo-V-based SCR catalysts with different calcination temperatures were tested under a simulated flue gas and the test results are exhibited in Fig. 3. For Hg^0 oxidation, when the calcination temperatures were 400 and 500 °C, it showed the highest Hg^0 oxidation activity (~53% at 5 ppmv HCl and ~69% at 10 ppmv HCl). With calcination temperature increasing to 600 °C, the Hg^0 oxidation conversion was reduced to 39% at 5 ppmv HCl and 55% at 10 ppmv HCl, respectively. Once the calcination temperature was enhanced to 700 °C, the modified catalyst almost lost the capability to oxidize Hg^0. For NO reduction, all of the catalysts showed the comparable NO reduction activity of ~80% at all calcination temperatures except at 700 °C showing the lowest NO reduction activity of ~54%. Therefore, lower temperature of 400 or 500 °C would be an optimal calcination temperature for synthesizing the Mo-V-based SCR catalyst. The effects of calcination temperatures were studied using multiple characterization techniques in Section 3.3.

3.2. Effects of experimental conditions on activities of Hg(0) oxidation and NO reduction

The activities of MoO_3+WO_3→V_2O_5/TiO_2 DT-51 CT500 prepared using anatase TiO_2 DT-51 as the support and 500 °C as the calcination temperature were investigated in terms of flue gas constituents, gas velocities, and reaction temperatures using a fixed-bed reactor system.

3.2.1. Effect of O_2

O_2 plays a significant part during the catalytic process. The effects of O_2 on simultaneous Hg^0 oxidation and NO reduction are shown in Fig.4. With an O_2 concentration increasing from 3 to 9%(v), Hg^0 oxidation activity enhanced from 69% to 81%. It demonstrated that O_2 was crucial to Hg^0 oxidation and had a positive effect. This result clearly shows that O_2 is required for Hg^0 oxidation. However, considering a typical range of ~3-6% O_2 concentrations existing in coal combustion flue gas, the impact of O_2 concentration was not significant. Meanwhile, NO reduction activity was ~80% with respect to different O_2 concentrations.

3.2.2. Effect of SO_2

When SO_2 concentration was raised from 200 to 2,000 ppmv, the catalytic activities of Hg^0 oxidation and NO reduction did not significantly change as shown in Fig.5. This means that the modified SCR catalyst is very robust and can be used in a wide range of SO_2 concentrations.

3.2.3. Effect of molar ratio of NH_3 to NO

NH_3/NO molar ratio is an important factor affecting Hg^0 oxidation and NO reduction activities because NH_3 can competitively adsorb with HCl. A ratio between 0 and 1.1 is used in the field to minimize an NH_3 slip of <5 ppm to avoid the formation of ammonium sulfate.[36, 37] The effects of NH_3/NO molar ratio on the simultaneous removal activities of Hg^0 and NO over MoO_3+WO_3→V_2O_5/TiO_2 DT-51 CT500 catalyst were tested under a simulated flue gas and the test results are exhibited in Fig. 6. When an NH_3/NO molar ratio increased over the range of 0.3 to 0.9, the Hg^0 oxidation activity was almost constant or slightly decreased from 73% to 69% (Fig. 6 (a)). However, with a further increase from 0.9 to 1.1, the Hg^0 oxidation activity significantly started to decrease from 69% to 59%. On the other hand, as NH_3/NO molar ratio increased from 0 to 1.1, the NO reduction activity almost linearly enhanced from 0 to 95%. The NO reduction

activity is found to be almost primarily dependent on the NH_3/NO molar ratio and to be insensitive to the rest of the parameters studied above.

3.2.4. Effect of GHSV

The effects of GHSV on the simultaneous removal activities of Hg^0 and NO over MoO_3+WO_3→V_2O_5/TiO_2 DT-51 CT500 catalyst were tested under the same combustion flue gas conditions and the test results are exhibited in Fig. 7. With a decrease in the GHSV from 40,000 hr^{-1} to 5,000 hr^{-1}, the Hg^0 oxidation activities enhanced from 53% to 93% at 5 ppmv HCl and from 69% to 99% at 10 ppmv HCl under the flue gas conditions. On the other hand, the NO reduction activities slightly increased from ~80% to 87% over a range of 5-10 ppmv HCl. It shows that the space velocity has an obvious impact on Hg^0 oxidation.

3.2.5. Effect of temperature

A typical operating temperature window of the SCR unit is between 300-400 °C in coal-fired power plants. The activities of simultaneous Hg^0 oxidation and NO reduction over the Mo-V-based SCR catalyst were tested between 300 and 400 °C and the test results are exhibited in Fig. 8. With an increase in temperature from 300 °C to 400 °C, Hg^0 oxidation activities was reduced from 81% to 38%. It indicated that in the typical SCR operating temperature window, lower temperature was beneficial to oxidize Hg^0. Meantime, the NO reduction activities of this Mo-V-based SCR catalyst was quite constant at ~80% within the same temperature range. An in-house V-based SCR catalyst V_2O_5+WO_3/TiO_2 DT-51 CT500 was also evaluated to compare with the Mo-V-based SCR catalyst. The conventional V-based SCR catalyst showed lower Hg^0 oxidation activities within a typical SCR operating temperature window between 300 and 400 °C. The activities difference in Hg^0 oxidation for these two catalyst samples decreased with an increase in temperature. Lower temperature could facilitate more HCl adsorption onto the catalyst surface

and thus Hg^0 oxidation could be kinetically limited by HCl adsorption.[24] The conventional V-based SCR catalyst also showed a comparable NO reduction activity at ~80%.

3.3. Characterization

3.3.1. BET

Since the activities were significantly different with respect to different TiO_2 supports and calcination temperatures, the BET surface area, pore volume and average pore diameter were examined by nitrogen adsorption-desorption isotherms as listed in Table 1. The catalyst samples with different TiO_2 supports showed slightly lower surface areas and pore volumes after doping metals. The loadings of V, Mo and W metals only insignificantly vary the surface areas and pore values of the Mo-V-based SCR catalysts with different TiO_2 supports. These BET surface area and pore volume values were still in the range of 36-120 m^2/g and 0.17-0.31 cm^3/g of typical SCR catalysts, respectively.[11, 15, 38]

The SCR catalyst sample prepared onto P25 had a surface area lower than that onto DT-51. The SCR catalyst sample onto rutile STR-100W had surface area, pore volume and size comparable to that onto anatase DT-51 although its activities were much lower (Fig. 2). Therefore, anatase phase TiO_2 was selected as a support for our Mo-V-based SCR catalyst.

When the calcination temperature of the samples onto anatase DT-51 was 400 and 500 ºC, the surface areas, pore volumes, and pore sizes were not significantly reduced. With the calcination temperature increasing to 600 ºC, they started to significantly decrease. At the calcination temperature of 700 ºC, they were almost close to zero. These results lead to additional examinations by images and X-ray-based techniques.

3.3.2. TEM

The images of TEM from the raw TiO_2 supports and Mo-V-based SCR catalysts based on different TiO_2 supports are shown in Fig. 9. After doping onto the support, the modified SCR catalyst samples retained almost the same physical structure as the raw supports, which was consistent with BET results. From the TEM images, some grain particles were found from the catalyst surfaces for all the three modified SCR catalysts (b, d, f). Since the loading quantity of V or W metals were rather lower than those needed to generate the theoretical monolayers, these grain particles are most likely derived from Mo as observed from previous studies.[28, 39, 40]

The TEM images of raw anatase DT-51 TiO_2 support and Mo-V-based SCR catalysts in terms of different calcination temperatures are exhibited in Fig. 10. The Mo-V-based SCR catalysts showed the morphological structure similar to the raw TiO_2 support when the calcination temperature was 400, 500 or 600 °C. The only difference was visible grain particles formed over the samples. With the calcination temperature increasing to 700 °C, the TiO_2 support particle dimension dramatically increased from ~30 nm to ~180 nm. Meanwhile, the small grain particles on the catalyst surface disappeared, suggesting that the calcination temperature of 700 °C led to the agglomeration of the support and the active metals. This is consistent with the very low surface area and pore volume of the sample prepared at 700 °C. The poor catalytic activities are very likely attributed to this agglomeration phenomenon taking place at 700 °C.

3.3.3. XRD

The XRD patterns of the raw TiO_2 (anatase DT-51, 75% anatase/25% rutile P25, and rutile STR-100W) supports and the catalyst samples synthesized at 500 °C are exhibited in Fig. 11. All the TiO_2 supports demonstrated their XRD patterns consistent with the information provided from the manufacture. All of the Mo-V-based SCR catalysts did not show any visible peaks for the

active metals, suggesting that they were likely in the amorphous phase or evenly spread over the TiO_2 support beyond the detection limit of XRD technique.[12]

The XRD patterns of the Mo-V-based SCR catalysts prepared on the anatase DT-51 TiO_2 support with respect to different calcination temperatures are exhibited in Fig. 12. For the Mo-V-based SCR catalysts synthesized at 400, 500 and 600 °C, no visible peaks for V_2O_5, MoO_3, and WO_3 were detected, suggesting the amorphous phase or uniform dispersion. Nevertheless, with the calcination temperature increasing to 700 ºC, the peaks at 27º, 36º, 41º, 44º, 54º and 57º belonging to the rutile phase were visible, indicating the transition from the anatase to rutile phase happened due to the high calcination temperature.[33-35] The phase transformation from anatase to rutile seems to lead to the major activities difference shown in Fig. 3. A peak at 23º was from MoO_3. At 700 ºC, small MoO_3 grain particles agglomerated into larger sizes, which was detectable by XRD. This could also lead to a negative impact on Hg^0 oxidation and NO reduction.

3.3.4. NH_3 TPD

The adsorption of NH_3 onto the catalyst surface is an important step during SCR process. Therefore, the surface acidity of the samples with different substrates was investigated using NH_3-TPD as shown in Fig. 13. For all of the three modified SCR catalysts with different TiO_2 supports, they all started to desorb NH_3 from ~60 °C. As temperature increased, the NH_3 desorption peak reached a maximum and then gradually decreased. Overall, the desorption of NH_3 occurred with a broad shape within a wide temperature range of ~60-450 °C. It indicated that several adsorbed NH_3 species with different thermal stability were present on the catalyst surface.

For the MoO_3+WO_3→V_2O_5/TiO_2 STR-100W CT500 catalyst, it showed ~0.18 mmol desorbed NH_3/g catalyst with a maximum NH_3 desorption peak at ~168 °C. However, the NH_3 species adsorbed onto the one with STR-100W was thermally unstable within a typical SCR

operating temperature range of ~300-400 °C and only a slight amount of NH_3 was desorbed in this temperature range. When DT-51 was used, a broader NH_3 desorption spectrum at higher temperatures was obtained. A total amount of NH_3 desorbed increased to ~0.23 mmol/g catalyst. More importantly, the sample showed higher thermal stability for adsorbed NH_3 between 300 and 400 °C, which could be used to reduce gaseous NO in the typical SCR operating temperature range. When P25 TiO_2 with 75% anatase and 25% rutile phases was used, the desorption spectrum showed a characteristic between anatase DT-51 and rutile STR-100W substrates with an estimated amount of NH_3 desorbed of ~0.18 mmol/g catalyst. More specifically, the desorbed amount of NH_3 at 350 °C were in the order of MoO_3+WO_3→V_2O_5/TiO_2 DT-51 CT500 > MoO_3+WO_3→V_2O_5/TiO_2 P25 CT500 > MoO_3+WO_3→V_2O_5/TiO_2 STR-100W CT500. These results are consistent with our NO reduction performance differences shown in Fig. 2.

3.3.5. XANES

Previous studies reported inconsistent results for V oxidation state changes using X-ray photoelectron spectroscopy (XPS) with respect to different calcination temperature.[41-44] In this study, XANES was employed to investigate the oxidation states and speciations of V from the fresh catalyst samples on different TiO_2 supports. Due to the interference between V and Ti, 0.5 wt.% V_2O_5 used in the Mo-V-based SCR formula was too low to conduct XAFS characterization. Therefore, V_2O_5 loading was raised from 0.5 to 2 wt.%. Fig. 14 exhibits V K-edge XANES spectra of the Mo-V-based SCR catalyst in terms of different TiO_2 supports with 2 wt.% V_2O_5 and vanadium oxide references . All the fresh catalyst samples had distinct pre-edge peaks, but the post-edge part was not differentiable. A comparison of the spectra of the catalyst samples with those of the V_2O_3, VO_2 and V_2O_5 standard samples suggests that the oxidation state of vanadium oxide consists of V^{5+} and V^{4+}.

To quantify the V oxidation states in the Mo-V-based SCR catalysts, linear combination fitting (LCF) analysis was employed. The derivative XANES spectra and LCF results are exhibited in Fig. 15, and the quantitative speciation data acquired are summarized in Table 2. The spectrum of the V_2O_3 standard with V^{3+} was completely deviated from those of the catalyst samples during the LCF analysis, and thus the V_2O_3 standard was ruled out from the analysis. When the MoO_3+WO_3→V_2O_5/TiO_2 DT-51 CT500 spectrum (Fig. 15(a)) was fitted with those of the references, the vanadium oxides could comprise 53.1% V^{5+} and 46.9% V^{4+}. When P25 and STR-100W were chosen as the supports, the content of V^{5+} slightly decreased to 49.3% and 47.1%, respectively. It seems that TiO_2 supports could not lead to significant differences on vanadium oxidation state. The significant Hg^0 oxidation and NO reduction activity differences may not be derived from the vanadium oxidation state change with respect to different TiO_2 supports.

Fig. 16 exhibits V K-edge XANES spectra of the Mo-V-based SCR catalyst samples based on different calcination temperatures with 2 wt.% V_2O_5 and vanadium oxide references. LCF was employed to quantify the V oxidation states from the fresh Mo-V-based SCR catalysts with different calcination temperatures. The derivative XANES spectra and LCF results are shown in Fig. 17, and the quantitative speciation data acquired are summarized in Table 3. The analysis for the MoO_3+WO_3→V_2O_5/TiO_2 DT-51 CT 400 °C sample (Fig. 17(a)) showed 52.2% V^{5+} and 47.8% V^{4+}. When the calcination temperature increased to 500 °C, the content of V^{5+} slightly increased to 53.1%. However, as the calcination temperatures increased to 600 °C and 700 °C, the content of V^{5+} dramatically decreased to 43.9% and 34.3%, respectively. This is in agreement with the catalytic activity differences (Fig. 3). As the calcination temperature increased from 400 or 500 °C to 600 °C, the Hg^0 oxidation activities decreased from ~53% to ~39% at 5 ppmv HCl and from ~69% to ~55% at 10 ppmv HCl. When the calcination temperature was 700 °C, the catalyst almost

completely lost its Hg^0 oxidation activity and decreased NO reduction activity from ~80% to ~54%. During the Hg^0 oxidation and NO reduction process, V^{5+} was reduced to V^{4+} based on our previous proposed mechanism.[28] Low V^{5+}/V^{4+} ratio correlates with low catalytic activity with an increase in calcination temperature. In addition to the physical agglomeration (Fig. 10) and the anatase to rutile phase change in TiO_2 (Fig. 12) under different calcination temperatures, the significant activity difference could also be attributed to a change in the V oxidation state. Throughout this study, rutile-phase TiO_2 was found to degrade both Hg^0 oxidation and NO reduction activities. Previous studies reported that degraded NO reduction activity of V-based SCR catalyst over the rutile phase is very likely attributed to crystallographic misfit between V_2O_5 and rutile TiO_2.[45-48] Although low V^{5+}/V^{4+} ratio can help account for the degraded activities over rutile TiO_2, it is not currently well understood about the role of rutile TiO_2.

4. Conclusions

In this study, the effects of preparation parameters including TiO_2 supports and calcination temperatures for Mo-V-based SCR catalysts on simultaneous Hg^0 oxidation and NO reduction were systematically investigated for the first time. Among different TiO_2 supports (anatase DT-51, mixed anatase/rutile phase P25 and rutile STR-100W) and four different calcination temperatures (400, 500, 600 and 700 °C), a combination of anatase phase TiO_2 and the calcination temperatures of 400 °C and 500 °C showed the best activities of simultaneous Hg^0 oxidation and NO reduction. When rutile phase or the high calcination temperature of 700 °C was used to prepare the Mo-V-based SCR catalyst, the catalyst lost almost its capability to oxidize Hg^0 and decreased NO reduction activity by ~30%. Different TiO_2 phase showed noticeable differences in the morphology. The calcination temperature of 700 °C could lead to the TiO_2 phase transformation

from anatase to rutile and the agglomeration of active metals with TiO_2. The content of V^{5+} decreased with an increase in rutile TiO_2 content or calcination temperature.

Our Mo-V-based SCR catalyst using anatase TiO_2 as the support and 500 °C as the calcination temperature preferred lower reaction temperature in a typical SCR operating temperature of 300-400 °C. It showed good SO_2 resistance in a wide range tested up to 2,000 ppmv SO_2 under a simulated sub-bituminous and lignite coal combustion flue gas. O_2 had a positive impact on Hg^0 oxidation and NH_3 had a negative effect on Hg(0) oxidation. With the molar ratio of NH_3/NO in a range of 0 to 1.1, the Hg^0 oxidation activity decreased and NO reduction activity increased. An increase in GHSV could significantly enhance Hg^0 oxidation, but slightly improve NO reduction. When the low space velocity of 5,000 hr^{-1} was used, the Hg^0 oxidation activity could achieve up to 99% under a typical sub-bituminous and lignite coal combustion flue gas condition. Compared to an in-house conventional V-based SCR catalyst, our Mo-V-based SCR catalyst showed much higher Hg^0 oxidation activity and comparable NO reduction activity. It has the potential to meet the stringent regulations for mercury and NO emissions in coal combustion flue gas using Mo-V-based SCR catalyst in an existing SCR unit.

Acknowledgements

This study was supported by the National Science Foundation, NSF CAREER Grant # 1151017. The authors greatly appreciate their financial support. This research used resources of the Advanced Photon Source, an Office of Science User Facility operated for the U.S. Department of Energy (DOE) Office of Science by Argonne National Laboratory, and was supported by the U.S. DOE under Contract No. DE-AC02-06CH11357, and the Canadian Light Source and its funding partners.

References

[1] C. Wiedinmyer, H. Friedli, Mercury emission estimates from fires: An initial inventory for the United States, Environ. Sci. Technol., 41 (2007) 8092-8098.

[2] J.H. Pavlish, E.A. Sondreal, M.D. Mann, E.S. Olson, K.C. Galbreath, D.L. Laudal, S.A. Benson, Status review of mercury control options for coal-fired power plants, Fuel Process. Technol., 82 (2003) 89-165.

[3] R. Meij, The fate of mercury in coal-fired power plants and the influence of wet flue-gas desulphurization, Water Air Soil Pollut., 56 (1991) 21-33.

[4] M.A. Abu-Daabes, N.G. Pinto, Synthesis and characterization of a nano-structured sorbent for the direct removal of mercury vapor from flue gases by chelation, Chemical Engineering Science, 60 (2005) 1901-1910.

[5] A.P. Jones, J.W. Hoffmann, D.N. Smith, T.J. Feeley, J.T. Murphy, DOE/NETL's phase II mercury control technology field testing program: preliminary economic analysis of activated carbon injection, Environ Sci Technol, 41 (2007) 1365-1371.

[6] Y. Zhuang, J.S. Thompson, C.J. Zygarlicke, J.H. Pavlish, Impact of calcium chloride addition on mercury transformations and control in coal flue gas, Fuel, 86 (2007) 2351-2359.

[7] Y. Yang, W. Xu, Y. Wu, J. Xiong, T. Zhu, X. Zhou, L. Tong, Effect of HBr formation on mercury oxidation via $CaBr_2$ addition to coal during combustion, RSC Adv., 6 (2016) 59009-59015.

[8] Q. Zhou, Y.-F. Duan, S.-L. Zhao, H.-F. Du, C. Zhu, M. She, H.-Q. Wei, Mercury transformation and NO emission of coal combustion with $CaCl_2$ and NH_4Cl additives in a 6 kW CFB combustor, Energy & Fuels, 29 (2015) 5267-5273.

[9] Y. Cao, Z. Gao, J. Zhu, Q. Wang, Y. Huang, C. Chiu, B. Parker, P. Chu, W. Pan, Impacts of Halogen Additions on Mercury Oxidation, in A Slipstream Selective Catalyst Reduction (SCR), Reactor When Burning Sub-Bituminous Coal, Environ. Sci. Technol., 42 (2007) 256-261.

[10] Y. Zhuang, J. Laumb, R. Liggett, M. Holmes, J. Pavlish, Impacts of acid gases on mercury oxidation across SCR catalyst, Fuel Process. Technol., 88 (2007) 929-934.

[11] S. He, J. Zhou, Y. Zhu, Z. Luo, M. Ni, K. Cen, Mercury oxidation over a vanadia-based selective catalytic reduction catalyst, Energy Fuels, 23 (2009) 253-259.

[12] L. Casagrande, L. Lietti, I. Nova, P. Forzatti, A. Baiker, SCR of NO by NH_3 over TiO_2-supported V_2O_5–MoO_3 catalysts: reactivity and redox behavior, Applied Catalysis B: Environmental, 22 (1999) 63-77.

[13] I. Nova, L. Lietti, L. Casagrande, L. Dall'Acqua, E. Giamello, P. Forzatti, Characterization and reactivity of TiO_2-supported MoO_3 De-NO_x SCR catalysts, Applied Catalysis B: Environmental, 17 (1998) 245-258.

[14] G. Busca, L. Lietti, G. Ramis, F. Berti, Chemical and mechanistic aspects of the selective catalytic reduction of NO_x by ammonia over oxide catalysts: a review, Applied Catalysis B: Environmental, 18 (1998) 1-36.

[15] H. Kamata, S. Ueno, T. Naito, A. Yukimura, Mercury Oxidation over the $V_2O_5(WO_3)/TiO_2$ Commercial SCR Catalyst, Ind Eng Chem Res, 47 (2008) 8136-8141.

[16] S. Niksa, N. Fujiwara, A Predictive Mechanism for Mercury Oxidation on Selective Catalytic Reduction Catalysts under Coal-Derived Flue Gas, J. Air & Waste Manage. Assoc., 55 (2005) 1866-1875.

[17] H. Li, C. Wu, Y. Li, J. Zhang, Superior activity of MnO_x-CeO_2/TiO_2 catalyst for catalytic oxidation of elemental mercury at low flue gas temperatures, Applied Catalysis B: Environmental, 111 (2012) 381-388.

[18] J. Zhou, W. Hou, P. Qi, X. Gao, Z. Luo, K. Cen, CeO_2-TiO_2 Sorbents for the Removal of Elemental Mercury from Syngas, Environ. Sci. Technol., 47 (2013) 10056-10062.

[19] L. Zhao, C. Li, J. Zhang, X. Zhang, F. Zhan, J. Ma, G. Zeng, Promotional effect of CeO_2 modified support on V_2O_5–WO_3/TiO_2 catalyst for elemental mercury oxidation in simulated coal-fired flue gas, Fuel, 153 (2015) 361-369.

[20] N. Yan, W. Chen, J. Chen, Z. Qu, Y. Guo, S. Yang, J. Jia, Significance of RuO_2 Modified SCR Catalyst for Elemental Mercury Oxidation in Coal-fired Flue Gas, Environ. Sci. Technol., 45 (2011) 5725-5730.

[21] Z. Liu, C. Li, V. Sriram, J.-Y. Lee, D. Brewe, XANES study of elemental mercury oxidation over RuO_2/TiO_2 and selective catalytic reduction catalysts for mercury emissions control, Fuel Processing Technology, 153 (2016) 156-162.

[22] Z. Liu, V. Sriram, C. Li, J.-Y. Lee, Mechanistic and kinetic studies of elemental mercury oxidation over a RuO_2/rutile TiO_2 catalyst, Catal. Sci. Technol., 7 (2017) 4669-4679.

[23] V. Sriram, C. Li, Z. Liu, M. Jafari, J.-Y. Lee, Reaction kinetic study of elemental mercury vapor oxidation with $CuCl_2$, Chemical Engineering Journal, 343 (2018) 244-257.

[24] H. Wang, B. Wang, Q. Sun, Y. Li, W.Q. Xu, J. Li, New insights into the promotional effects of Cu and Fe over V_2O_5-WO_3/TiO_2 NH_3-SCR catalysts towards oxidation of Hg^0, Catalysis Communications, (2017).

[25] B. Zhao, X. Liu, Z. Zhou, H. Shao, C. Wang, J. Si, M. Xu, Effect of molybdenum on mercury oxidized by V_2O_5–MoO_3/TiO_2 catalysts, Chemical Engineering Journal, 253 (2014) 508-517.

[26] B. Zhao, J. Han, L. Qin, W. Chen, Z. Zhou, F. Xing, Impact of individual flue gas component on mercury oxidation over V_2O_5-MoO_3/TiO_2 catalyst, New J. Chem., 42 (2018) 20190-20196.

[27] B. Zhao, X.W. Liu, Z.J. Zhou, H.Z. Shao, C. Wang, M.H. Xu, Mercury oxidized by V_2O_5-MoO_3/TiO_2 under multiple components flue gas: An actual coal-fired power plant test and a laboratory experiment, Fuel Processing Technology, 134 (2015) 198-204.

[28] C. Li, D. Brewe, J.Y. Lee, Effects of impregnation sequence for Mo-modified V-based SCR catalyst on simultaneous Hg (0) oxidation and NO reduction, Appl. Catal. B, (2020) 118854.

[29] K. Nochi, M. Yonemura, M. Kiyosawa, Mercury oxidation catalyst and method for producing the same, US 8288309 B2, Washington, DC: U.S. Patent and Trademark Office, 2012.

[30] J. Regalbuto, Catalyst Preparation: Science and Engineering, CRC Press, 2007.

[31] L.J. Alemany, F. Berti, G. Busca, G. Ramis, D. Robba, G.P. Toledo, M. Trombetta, Characterization and composition of commercial V_2O_5-WO_3-TiO_2 SCR catalysts, Applied Catalysis B: Environmental, 10 (1996) 299-311.

[32] J. Chen, R. Yang, Selective catalytic reduction of NO with NH_3 on SO_4^{-2}/TiO_2 superacid catalyst, Journal of Catalysis, 139 (1993) 277-288.

[33] J. Kim, K.C. Song, S. Foncillas, S.E. Pratsinis, Dopants for synthesis of stable bimodally porous titania, Journal of the European Ceramic Society, 21 (2001) 2863-2872.

[34] J. Ovenstone, K. Yanagisawa, Effect of Hydrothermal Treatment of Amorphous Titania on the Phase Change from Anatase to Rutile during Calcination, Chem. Mater., 11 (1999) 2770-2774.

[35] J. Zhang, Q. Xu, Z. Feng, M. Li, C. Li, Importance of the Relationship between Surface Phases and Photocatalytic Activity of TiO_2, Angew. Chem. Int. Ed., 47 (2008) 1766-1769.

[36] H. Gutberlet, B. Schallert, Selective catalytic reduction of NO_x from coal fired power plants Catalysis Today, 16 (1993) 207-236.

[37] I.Y. Lee, D.W. Kim, J.B. Lee, K.O. Yoo, A practical scale evaluation of sulfated V_2O_5/TiO_2 catalyst from metatitanic acid for selective catalytic reduction of NO by NH_3, Chemical Engineering Journal, 90 (2002) 267-272.

[38] Z.Y. Liu, V. Sriram, J.Y. Lee, Heterogeneous oxidation of elemental mercury vapor over RuO_2/rutile TiO_2 catalyst for mercury emissions control, Applied Catalysis B: Environmental, 207 (2017) 143-152.

[39] G. Deo, I.E. Wachs, Reactivity of Supported Vanadium Oxide Catalysts: The Partial Oxidation of Methanol, Journal of Catalysis, 146 (1994) 323-334.

[40] I.E. Wachs, Raman and IR studies of surface metal oxide species on oxide supports: Supported metal oxide catalysts, Catalysis Today, 27 (1996) 437-455.

[41] B.M. Reddy, P. Lakshmanan, A. Khan, Investigation of surface structures of dispersed V_2O_5 on CeO_2−SiO_2, CeO_2−TiO_2, and CeO_2−ZrO_2 mixed oxides by XRD, Raman, and XPS techniques, The Journal of Physical Chemistry B, 108 (2004) 16855-16863.

[42] X. Gu, J. Ge, H. Zhang, A. Auroux, J. Shen, Structural, redox and acid–base properties of V_2O_5/CeO_2 catalysts, Thermochimica Acta, 451 (2006) 84-93.

[43] B.M. Reddy, K.N. Rao, G.K. Reddy, P. Bharali, Characterization and catalytic activity of V_2O_5/Al_2O_3-TiO_2 for selective oxidation of 4-methylanisole, Journal of Molecular Catalysis A: Chemical, 253 (2006) 44-51.

[44] B.M. Reddy, B. Chowdhury, I. Ganesh, E. Reddy, T. Rojas, A. Fernandez, Characterization of $V_2O_5/TiO_2{-}ZrO_2$ catalysts by XPS and other techniques, The Journal of Physical Chemistry B, 102 (1998) 10176-10182.

[45] A. Vejux, P. Courtine, Interfacial Reactions between V_2O_5 and TiO_2 (Anatase): Role of the Structural Properties, Journal of Solid State Chemistry, 23 (1978) 93-103.

[46] N.N. Nair, T. Bredow, K. Jug, Toward an Understanding of the Formation of Vanadia−Titania Catalysts, The Journal of Physical Chemistry B, 109 (2005) 12115-12123.

[47] G. Centi, E. Giamello, D. Pinelli, F. Trifiro, Surface structure and reactivity of V-Ti-O catalysts prepared by solid-state reaction 1. Formation of a V^{IV} interacting layer, Journal of Catalysis, 130 (1991) 220-237.

[48] J.W. Choung, I.-S. Nam, S.-W. Ham, Effect of promoters including tungsten and barium on the thermal stability of V_2O_5/sulfated TiO_2 catalyst for NO reduction by NH_3, Catalysis Today, 111 (2006) 242-247.

Table captions

Table 1. BET surface area, pore volume and average pore diameter measurements for Mo-V-based SCR catalysts.

Table 2. LCF results for vanadium species of Mo-V-based SCR catalysts with different TiO_2 supports.

Table 3. LCF results for vanadium species of Mo-V-based SCR catalysts with respect to different calcination temperatures.

Table 1. BET surface area, pore volume and average pore diameter measurements for Mo-V-based SCR catalysts.

Catalyst	BET surface area (m^2/g)	Pore volume (cm^3/g)	Average pore diameter (nm)
TiO_2 (DT-51)*	72	0.38	20.2
TiO_2 (P25)	51	0.31	24.8
TiO_2 (STR-100W)	67	0.37	22.4
MoO_3+WO_3→V_2O_5/TiO_2 DT-51 CT500*	65	0.26	15.7
MoO_3+WO_3→V_2O_5/TiO_2 P25 CT500	42	0.27	26.2
MoO_3+WO_3→V_2O_5/TiO_2 STR-100W CT500	62	0.33	27.7
MoO_3+WO_3→V_2O_5/TiO_2 DT-51 CT400	69	0.25	14.3
MoO_3+WO_3→V_2O_5/TiO_2 DT-51 CT600	48	0.21	17.7
MoO_3+WO_3→V_2O_5/TiO_2 DT-51 CT700	5	0.01	8.9

Note: *[28]; CT: calcination temperature

Table 2. LCF results for vanadium species of Mo-V-based SCR catalysts with different TiO_2 supports.

Samples	V_2O_5 (V^{5+}) (%)	VO_2 (V^{4+}) (%)	Ratio of V^{5+} to V^{4+}
Fresh MoO_3+WO_3→V_2O_5/TiO_2 DT-51 CT500*	53.1 ± 2.0	46.9 ± 2.0	1.13
Fresh MoO_3+WO_3→V_2O_5/TiO_2 P25 CT500	49.3 ± 2.2	50.7 ± 2.2	0.97
Fresh MoO_3+WO_3→V_2O_5/TiO_2 STR-100W CT500	47.1 ± 2.3	52.9 ± 2.3	0.89

Note: *[28]

Table 3. LCF fitting results for vanadium species of Mo-V-based SCR catalysts with respect to different calcination temperatures.

Samples	V_2O_5 (V^{5+}) (%)	VO_2 (V^{4+}) (%)	Ratio of $V^{5+}$to V^{4+}
Fresh MoO_3+WO_3→V_2O_5/TiO_2 DT-51 CT400	52.2 ± 2.8	47.8 ± 2.8	1.09
Fresh MoO_3+WO_3→V_2O_5/TiO_2 DT-51 CT500	53.1 ± 2.0	46.9 ± 2.0	1.13
Fresh MoO_3+WO_3→V_2O_5/TiO_2 DT-51 CT600	43.9 ± 2.6	56.1 ± 2.6	0.78
Fresh MoO_3+WO_3→V_2O_5/TiO_2 DT-51 CT700	34.3 ± 1.8	65.7 ± 1.8	0.52

Figure captions

Fig. 1. Schematic of lab-scale fixed-bed reactor set-up.

Fig. 2. Activity test results of Mo-V-based SCR catalysts for Hg^0 oxidation (a) and NO reduction (b) in terms of different TiO_2 supports (DT-51*, P25 and STR-100W). Experimental conditions: 15 ppbv Hg^0, 300 ppmv NO, 270 ppmv NH_3 (molar ratio of NH_3 to NO=0.9), 200 ppmv SO_2, 3%(v) O_2, 10%(v) H_2O, 12%(v) CO_2 balanced with N_2 at T=350 °C and GHSV=40,000 hr^{-1}. Note: *[28].

Fig. 3. Activity test results of Mo-V-based SCR catalysts for Hg^0 oxidation (a) and NO reduction (b) in terms of different calcination temperatures (400, 500, 600 and 700 °C) . Experimental conditions: 15 ppbv Hg^0, 300 ppmv NO, 270 ppmv NH_3 (molar ratio of NH_3 to NO=0.9), 200 ppmv SO_2, 3%(v) O_2, 10%(v) H_2O, 12%(v) CO_2 balanced with N_2 at T=350 °C and GHSV=40,000 hr^{-1}.

Fig. 4. Effect of O_2 on simultaneous Hg^0 oxidation (a) and NO reduction (b) over Mo-V-based SCR catalyst MoO_3+WO_3→V_2O_5/TiO_2 DT-51 CT500. Experimental conditions: 15 ppbv Hg^0, 300 ppmv NO, 270 ppmv NH_3 (molar ratio of NH_3 to NO=0.9), 200 ppmv SO_2, 10 ppmv HCl, 10%(v) H_2O, 12%(v) CO_2 balanced with N_2 at T=350 ºC and GHSV=40,000 hr^{-1}.

Fig. 5. Effect of SO_2 on simultaneous Hg^0 oxidation (a) and NO reduction (b) over MoO_3+WO_3→V_2O_5/TiO_2 DT-51 CT500. Experimental conditions: 15 ppbv Hg^0, 300 ppmv NO, 270 ppmv NH_3 (molar ratio of NH_3 to NO=0.9), 3%(v) O_2, 10 ppmv HCl, 10%(v) H_2O, 12%(v) CO_2 balanced with N_2 at T=350 ºC and GHSV=40,000 hr^{-1}.

Fig. 6. Effect of NH_3/NO molar ratios on simultaneous Hg^0 oxidation (a) and NO reduction (b) over MoO_3+WO_3→V_2O_5/TiO_2 DT-51 CT500. Experimental conditions: 15 ppbv Hg^0, 300 ppmv

NO, 200 ppmv SO_2, 3%(v) O_2, 10 ppmv HCl, 10%(v) H_2O, 12%(v) CO_2 balanced with N_2 at T=350 ºC and GHSV=40,000 hr^{-1}.

Fig. 7. Effect of GHSV on simultaneous Hg^0 oxidation (a) and NO reduction (b) over MoO_3+WO_3→V_2O_5/TiO_2 DT-51 CT500. Experimental conditions: 15 ppbv Hg^0, 300 ppmv NO, 270 ppmv NH_3 (molar ratio of NH_3 to NO=0.9), 200 ppmv SO_2, 3%(v) O_2, 10%(v) H_2O, 12%(v) CO_2 balanced with N_2 at T=350 ºC.

Fig. 8. Effect of reaction temperatures on simultaneous Hg^0 oxidation (a) and NO reduction (b) over Mo-V-based SCR catalyst MoO_3+WO_3→V_2O_5/TiO_2 DT-51 CT500 and V_2O_5+WO_3/TiO_2 DT-51 CT500. Experimental conditions: 15 ppbv Hg^0, 300 ppmv NO, 270 ppmv NH_3 (molar ratio of NH_3 to NO=0.9), 200 ppmv SO_2, 3%(v) O_2, 10 ppmv HCl, 10%(v) H_2O, 12%(v) CO_2 balanced with N_2 and GHSV=40,000 hr^{-1}.

Fig. 9. TEM images of Mo-V-based SCR catalysts in terms of different TiO_2 supports: (a) TiO_2 (DT-51)*; (b) MoO_3+WO_3→V_2O_5/TiO_2 DT-51 CT500*; (c) TiO_2 (P25); (d) MoO_3+WO_3→V_2O_5/TiO_2 P25 CT500; (e) TiO_2 (STR-100W); (f) MoO_3+WO_3→V_2O_5/TiO_2 STR-100W CT500. Scale bars: 20 nm. Note: *[28].

Fig. 10. TEM images of Mo-V-based SCR catalysts in terms of different calcination temperatures: (a) TiO_2 (DT-51); (b) MoO_3+WO_3→V_2O_5/TiO_2 DT-51 CT400; (c) MoO_3+WO_3→V_2O_5/TiO_2 DT-51 CT500; (d) MoO_3+WO_3→V_2O_5/TiO_2 DT-51 CT600; (e) MoO_3+WO_3→V_2O_5/TiO_2 DT-51 CT700; (f) MoO_3+WO_3→V_2O_5/TiO_2 DT-51 CT700. All the scale bars are 20 nm except for (e) with 200 nm.

Fig. 11. XRD patterns of Mo-V-based SCR catalysts on different TiO_2 supports calcined at 500 °C: (a) Anatase TiO_2 DT-51*; (b) Anatase/rutile TiO_2 P25; (c) Rutile TiO_2 STR-100W; (d)

MoO_3+WO_3→V_2O_5/TiO_2 DT-51 CT500*; (e) MoO_3+WO_3→V_2O_5/TiO_2 P25 CT500; (f) MoO_3+WO_3→V_2O_5/TiO_2 STR-100W CT500. Note: *[28].

Fig. 12. XRD patterns of MoO_3+WO_3→V_2O_5/TiO_2 DT-51 with respect to different calcination temperatures: (a) Anatase TiO_2 DT-51; (b) Rutile TiO_2 STR-100W; (c) MoO_3+WO_3→V_2O_5/TiO_2 DT-51 CT400; (d) MoO_3+WO_3→V_2O_5/TiO_2 DT-51 CT500; (e) MoO_3+WO_3→V_2O_5/TiO_2 DT-51 CT600; (f) MoO_3+WO_3→V_2O_5/TiO_2 DT-51 CT700.

Fig. 13. NH_3-TPD spectra of Mo-V-based SCR catalysts with different TiO_2 supports (DT-51, P25 and STR-100W).

Fig. 14. Vanadium K-edge XANES spectra of Mo-V-based SCR catalyst samples with different TiO_2 supports (DT-51*, P25 and STR-100W) and standard reference vanadium oxide samples. Note: *[28].

Fig. 15. LCF results for vanadium species of Mo-V-based SCR catalysts with different TiO_2 supports: (a) Fresh MoO_3+WO_3→V_2O_5/TiO_2 DT-51 CT500*; (b) Fresh MoO_3+WO_3→V_2O_5/TiO_2 P25 CT500; (c) Fresh MoO_3+WO_3→V_2O_5/TiO_2 STR-100W CT500. Note: *[28].

Fig. 16. Vanadium K-edge XANES spectra of Mo-V-based SCR catalyst samples with respect to different calcination temperatures (400, 500, 600 and 700 ºC) and standard reference vanadium oxide samples.

Fig. 17. LCF results for vanadium species of Mo-V-based SCR catalysts with respect to different calcination temperatures: (a) Fresh MoO_3+WO_3→V_2O_5/TiO_2 DT-51 CT400; (b) Fresh

MoO_3+WO_3→V_2O_5/TiO_2 DT-51 CT500; (c) Fresh MoO_3+WO_3→V_2O_5/TiO_2 DT-51 CT600; (d) Fresh MoO_3+WO_3→V_2O_5/TiO_2 DT-51 CT700.

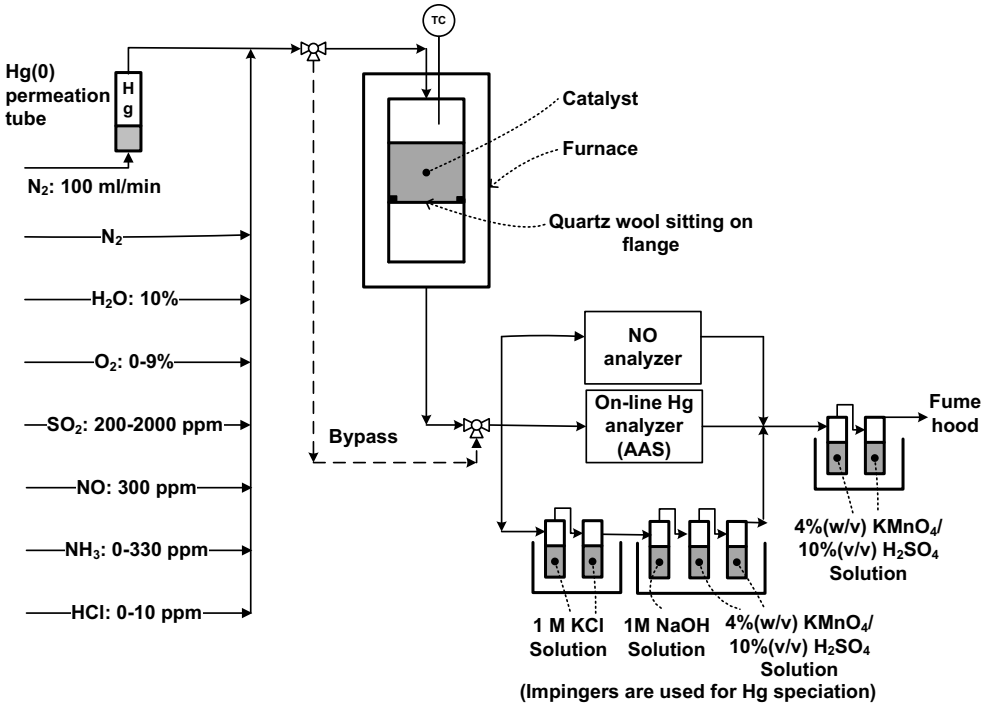

Fig. 1.

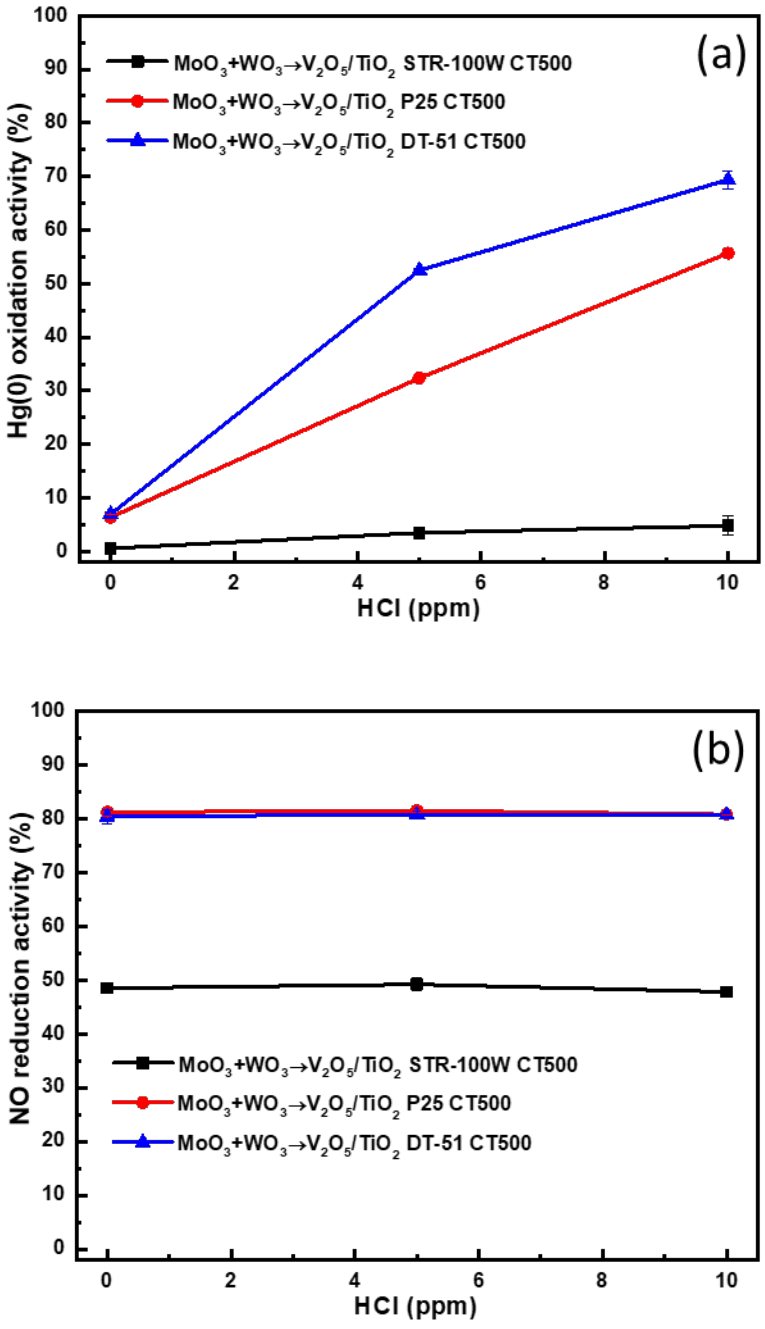
(a)
MoO3+WO3→V2O5/TiO2 STR-100W CT500
MoO3+WO3→V2O5/TiO2 P25 CT500
MoO3+WO3→V2O5/TiO2 DT-51 CT500
Hg(0) oxidation activity (%)
HCl (ppm)
(b)
NO reduction activity (%)
HCl (ppm)

Fig. 2.

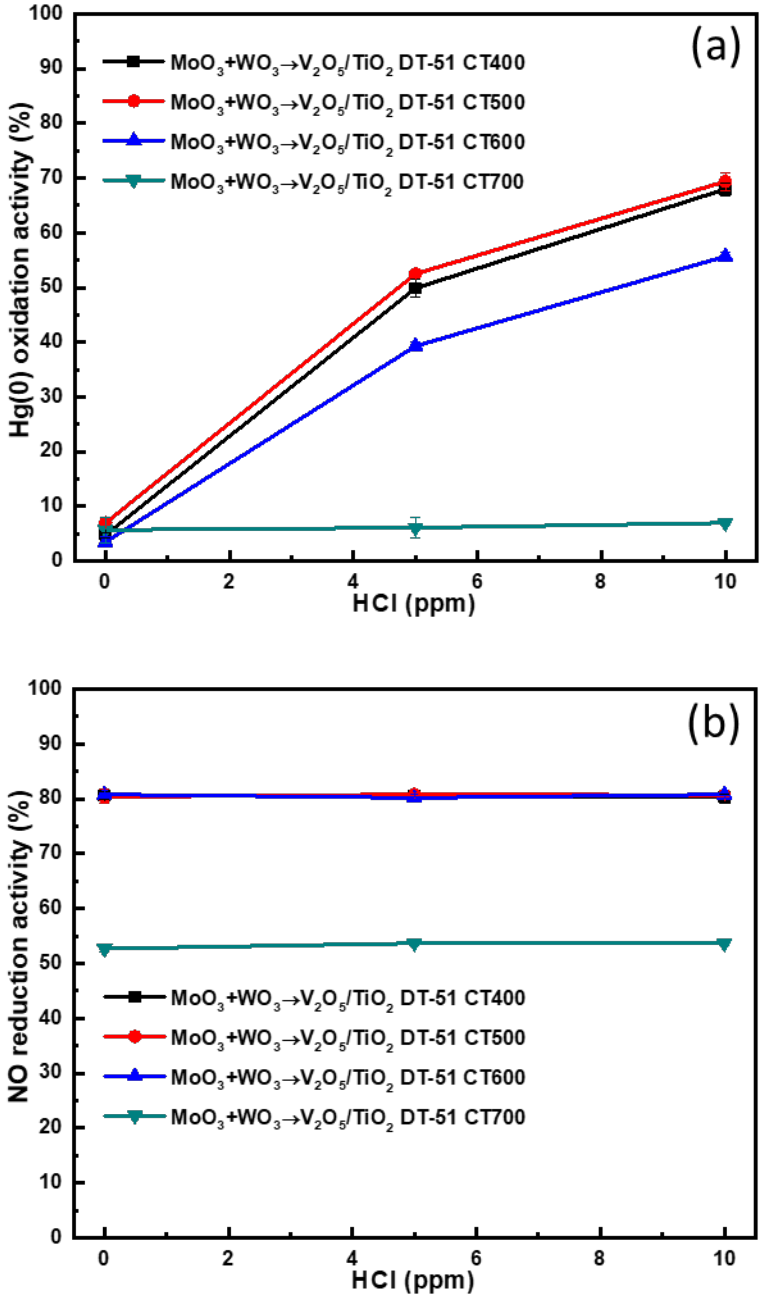
(a)
Hg(0) oxidation activity (%)
HCl (ppm)
MoO3+WO3→V2O5/TiO2 DT-51 CT400
MoO3+WO3→V2O5/TiO2 DT-51 CT500
MoO3+WO3→V2O5/TiO2 DT-51 CT600
MoO3+WO3→V2O5/TiO2 DT-51 CT700
(b)
NO reduction activity (%)
HCl (ppm)
MoO3+WO3→V2O5/TiO2 DT-51 CT400
MoO3+WO3→V2O5/TiO2 DT-51 CT500
MoO3+WO3→V2O5/TiO2 DT-51 CT600
MoO3+WO3→V2O5/TiO2 DT-51 CT700

Fig. 3.

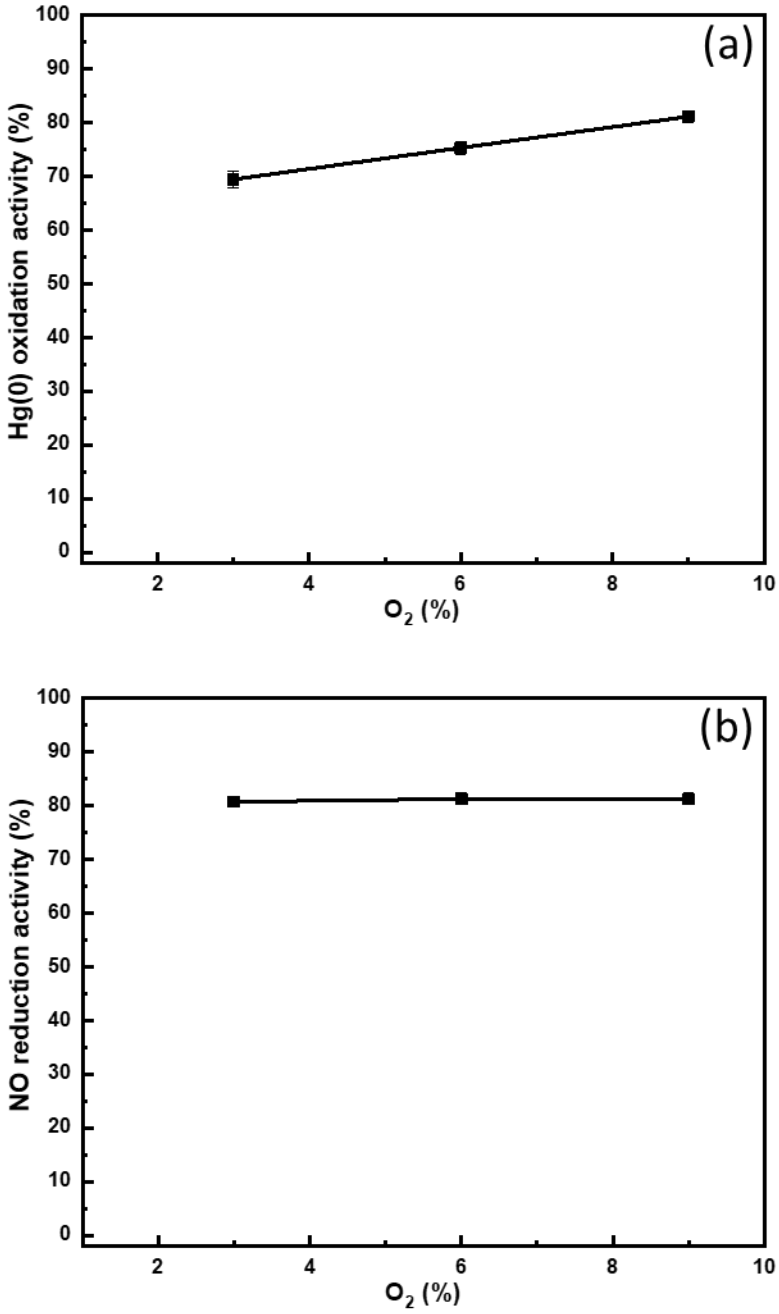
(a)
Hg(0) oxidation activity (%)
100
90
80
70
60
50
40
30
20
10
0
2
4
6
8
10
O2 (%)
(b)
NO reduction activity (%)
100
90
80
70
60
50
40
30
20
10
0
2
4
6
8
10
O2 (%)

Fig. 4.

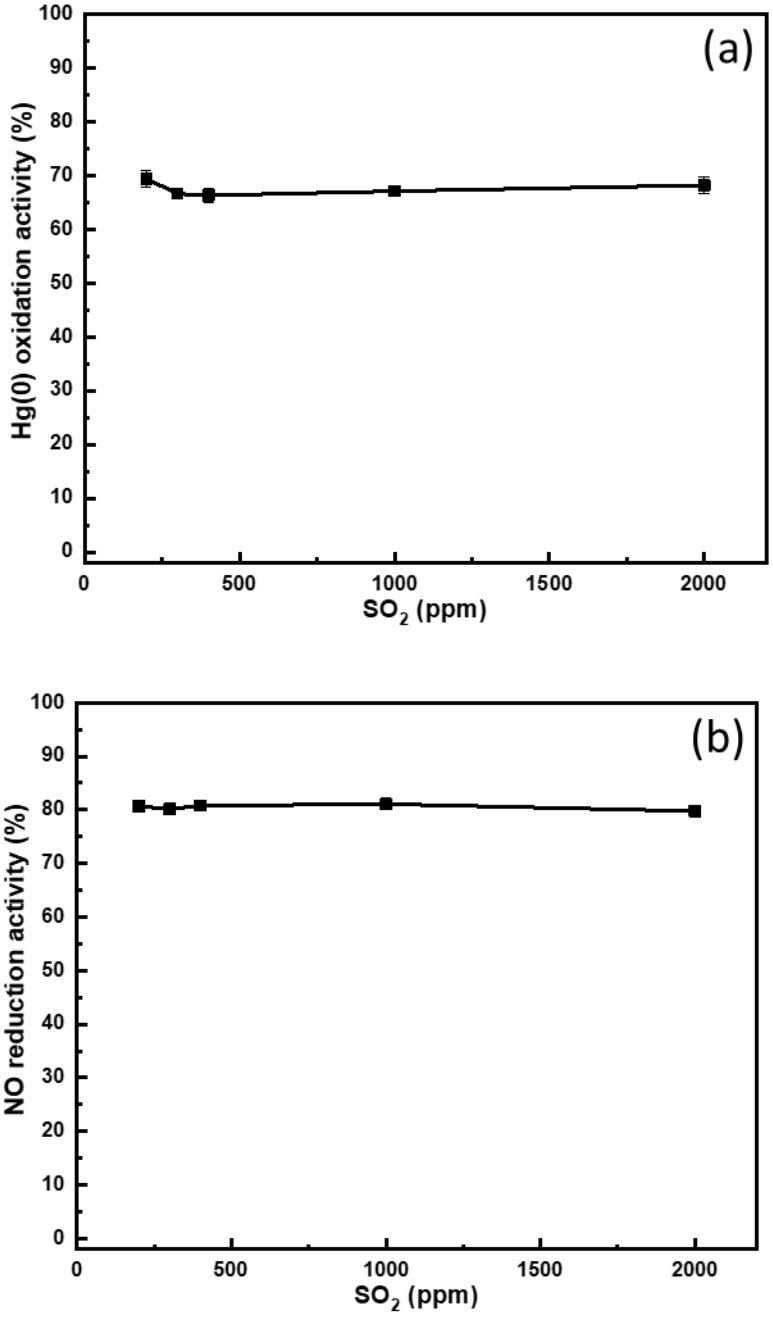
(a)
Hg(0) oxidation activity (%)
100
90
80
70
60
50
40
30
20
10
0
0
500
1000
1500
2000
SO2 (ppm)
(b)
NO reduction activity (%)
100
90
80
70
60
50
40
30
20
10
0
0
500
1000
1500
2000
SO2 (ppm)

Fig. 5.

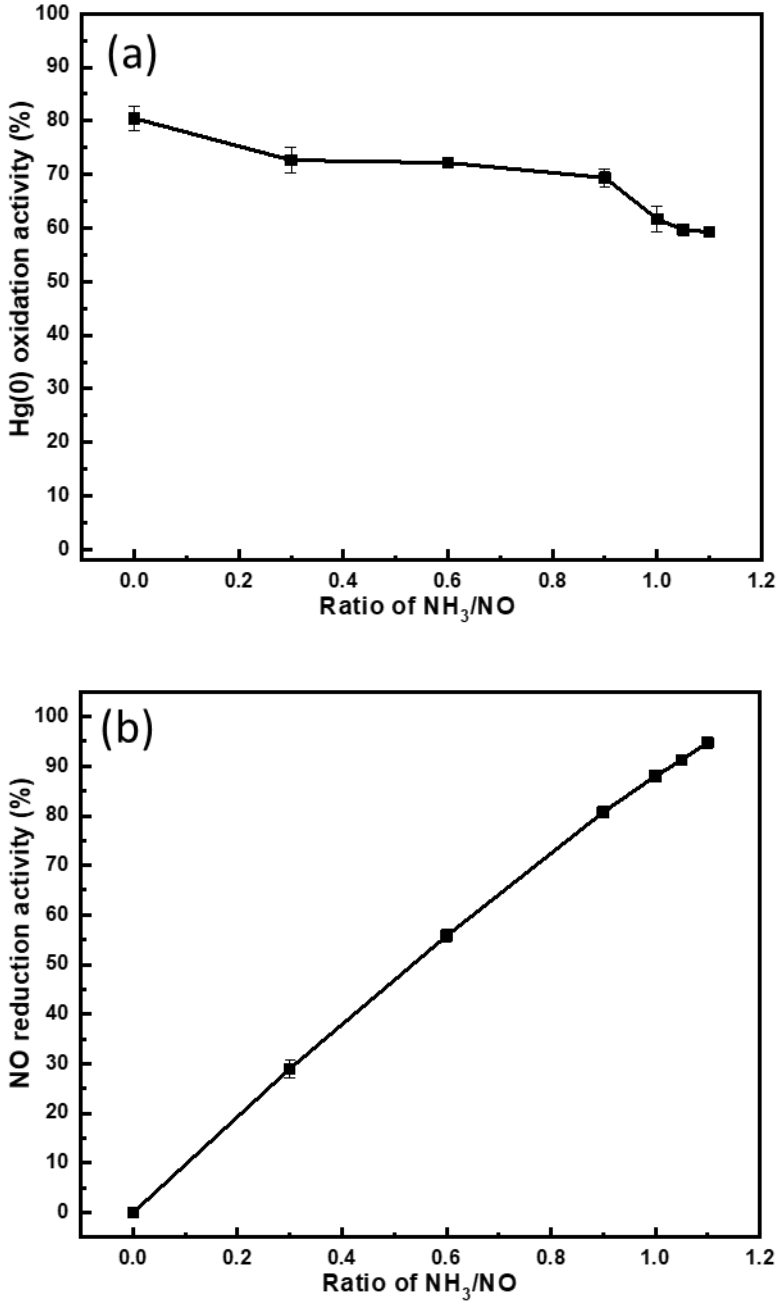
(a)
Hg(0) oxidation activity (%)
Ratio of NH3/NO
(b)
NO reduction activity (%)
Ratio of NH3/NO

Fig. 6.

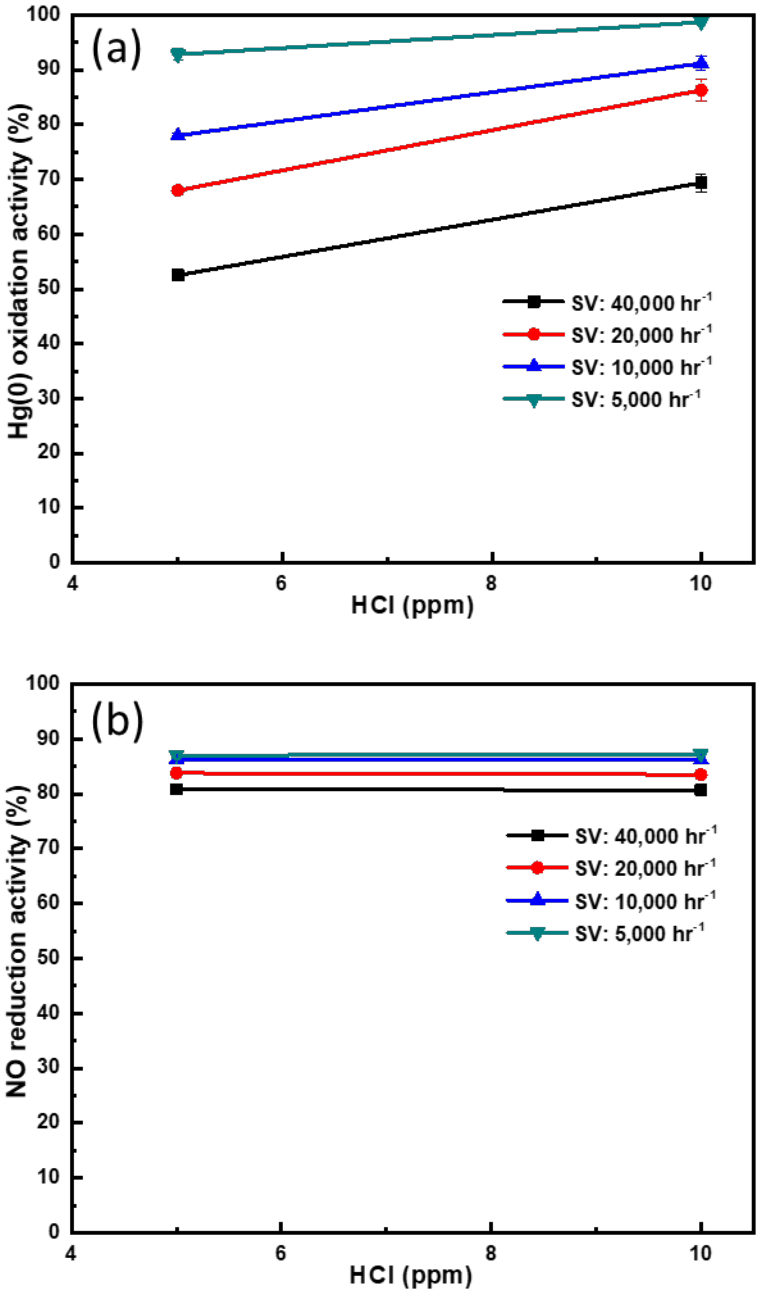
(a)
Hg(0) oxidation activity (%)
HCl (ppm)
SV: 40,000 hr-1
SV: 20,000 hr-1
SV: 10,000 hr-1
SV: 5,000 hr-1
(b)
NO reduction activity (%)
HCl (ppm)
SV: 40,000 hr-1
SV: 20,000 hr-1
SV: 10,000 hr-1
SV: 5,000 hr-1

Fig. 7.

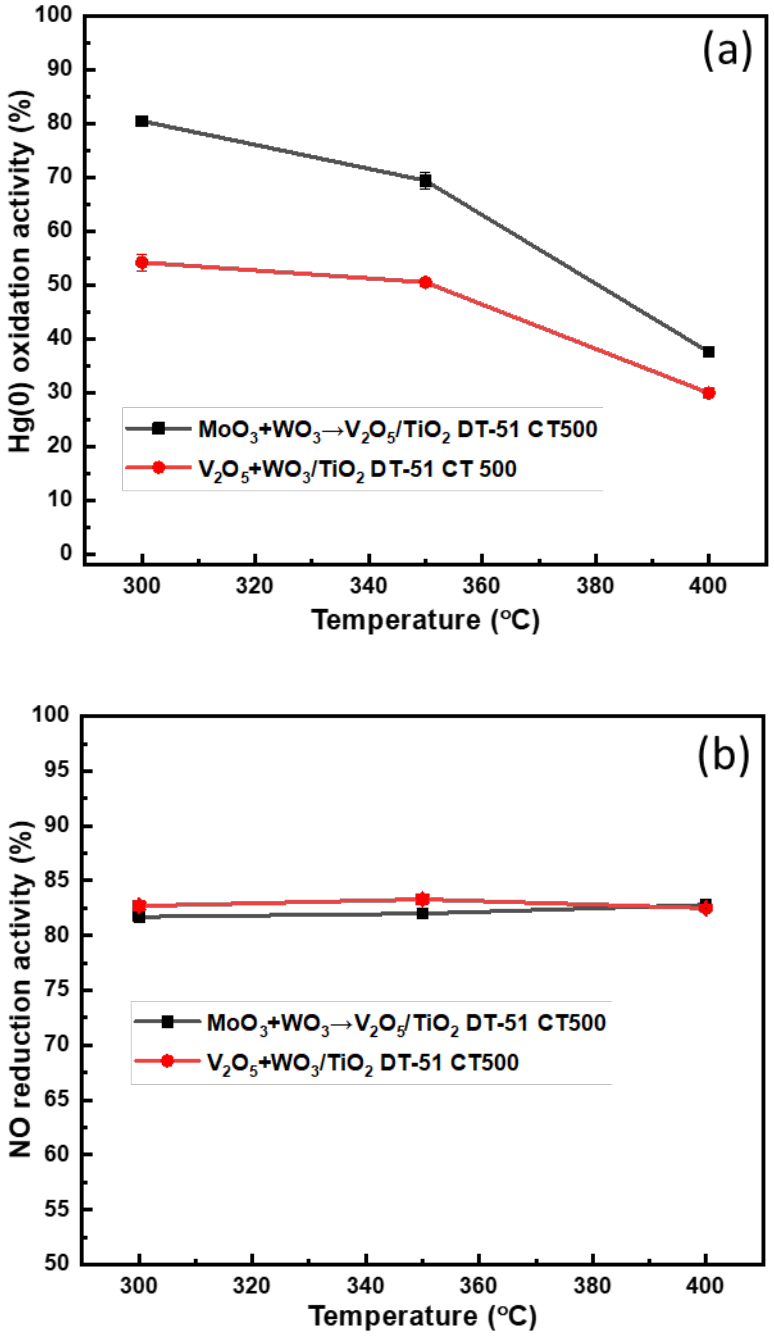
(a)
Hg(0) oxidation activity (%)
Temperature (°C)
MoO3+WO3→V2O5/TiO2 DT-51 CT500
V2O5+WO3/TiO2 DT-51 CT 500
(b)
NO reduction activity (%)
Temperature (°C)
MoO3+WO3→V2O5/TiO2 DT-51 CT500
V2O5+WO3/TiO2 DT-51 CT500

Fig. 8.

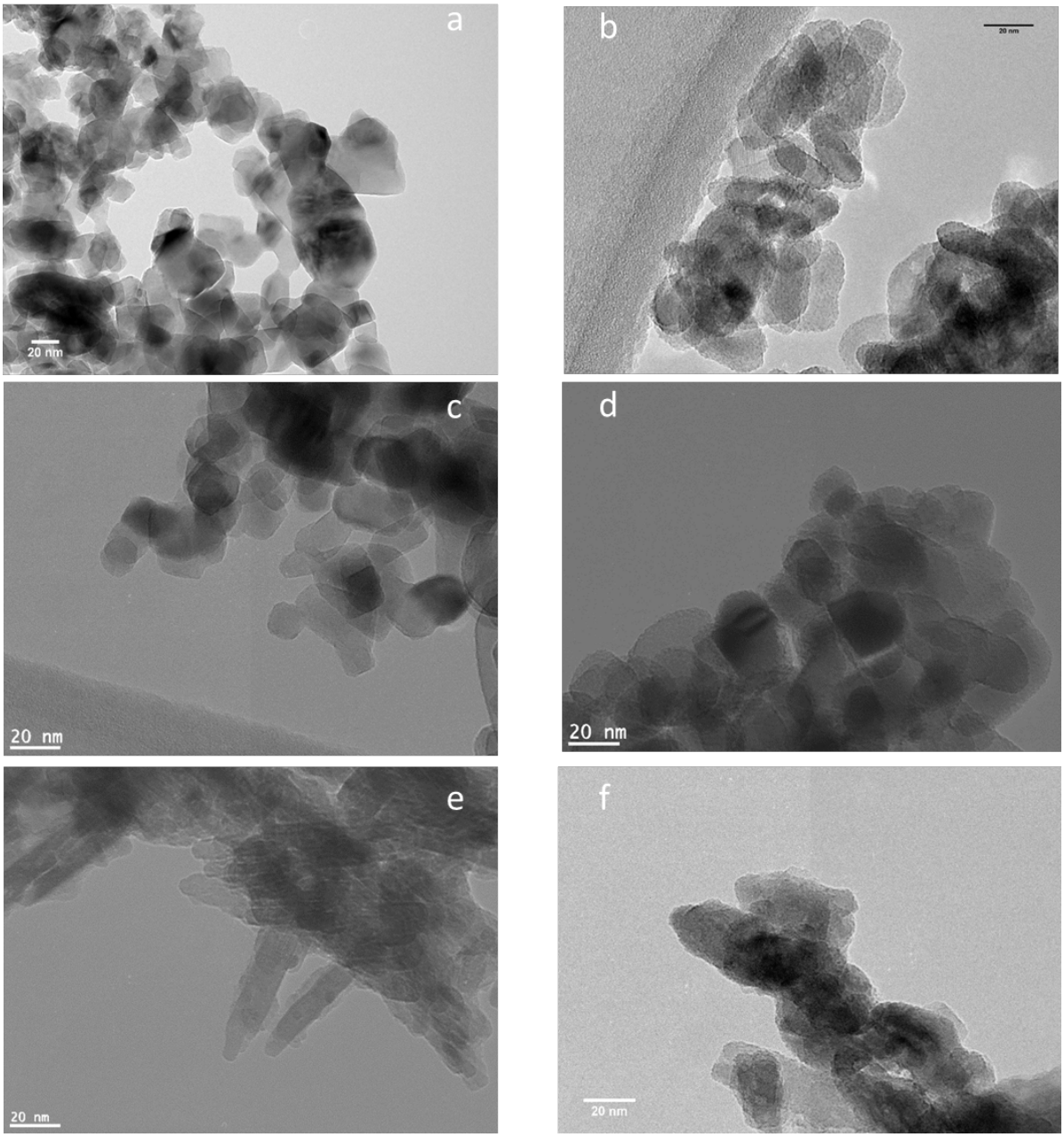

Fig. 9.

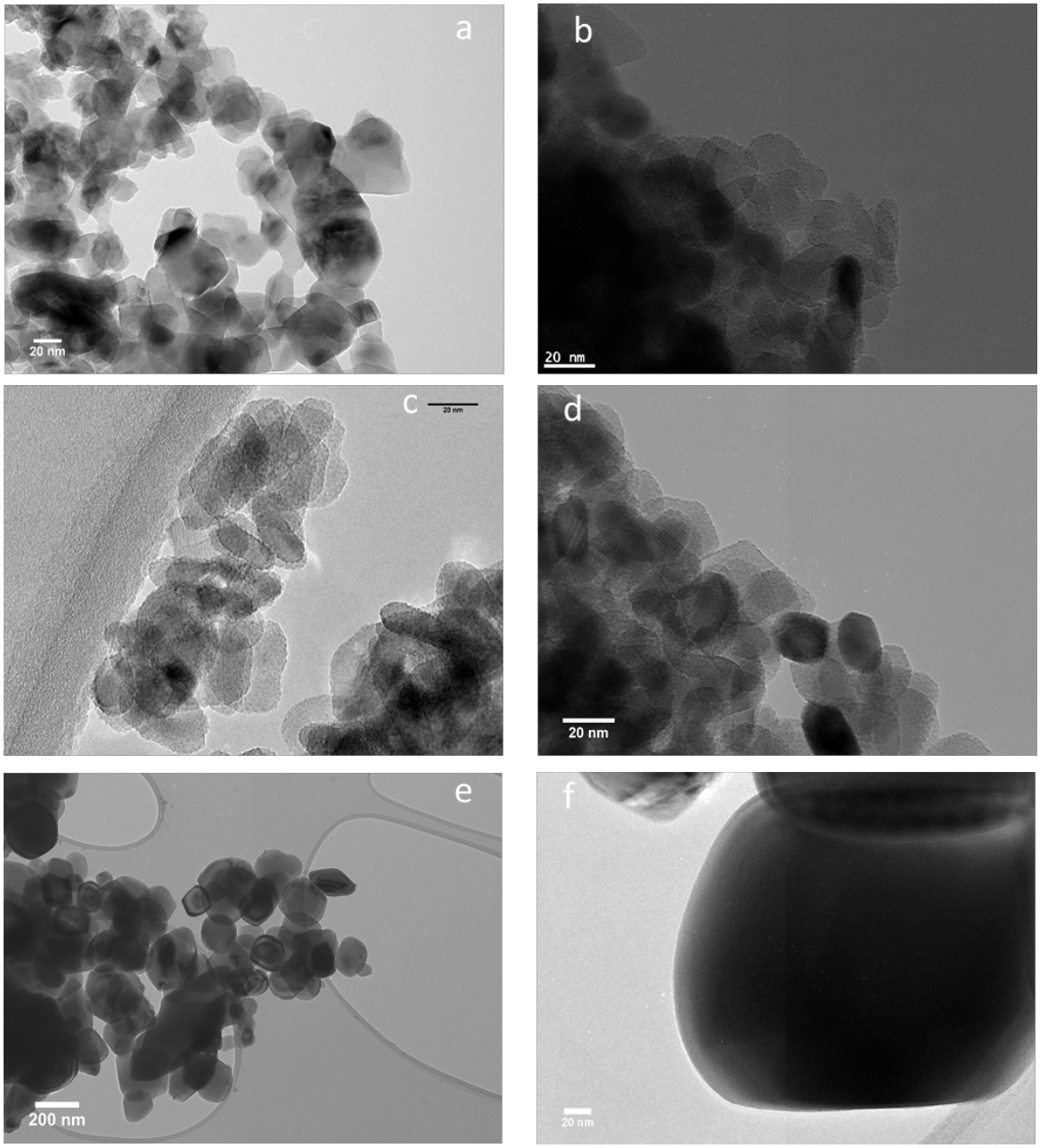

Fig. 10.

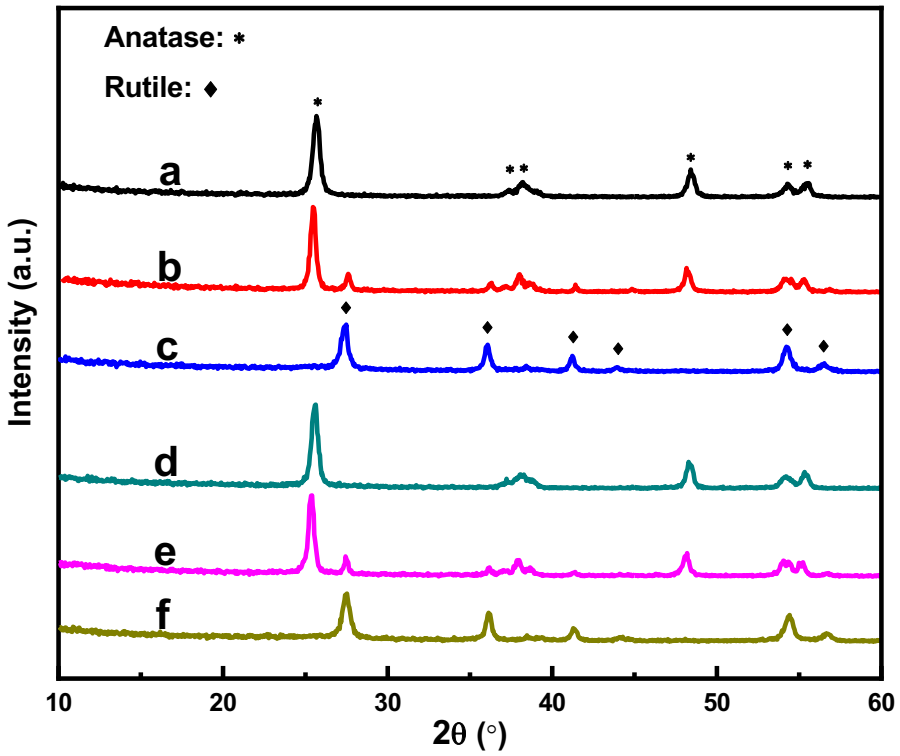

Fig. 11.

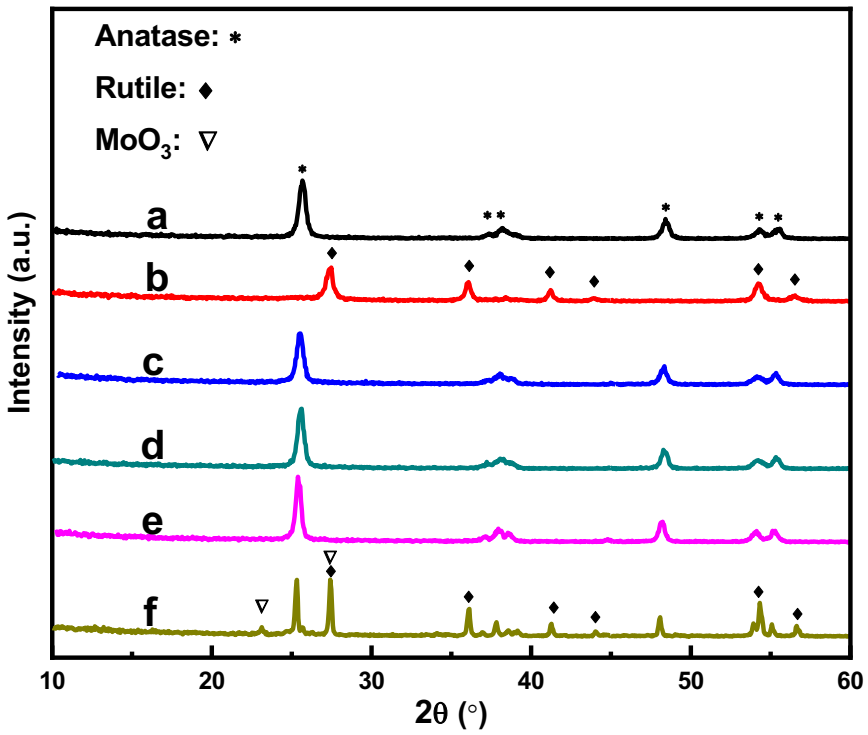

Fig. 12.

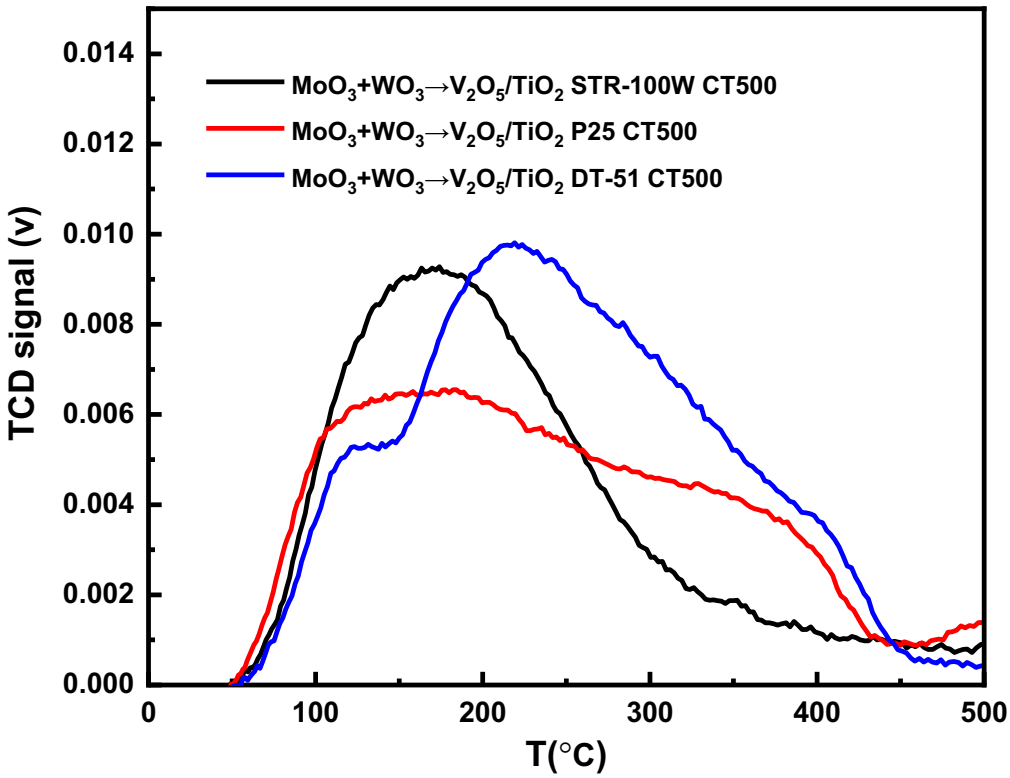
MoO3+WO3→V2O5/TiO2 STR-100W CT500
MoO3+WO3→V2O5/TiO2 P25 CT500
MoO3+WO3→V2O5/TiO2 DT-51 CT500
TCD signal (v)
0.014
0.012
0.010
0.008
0.006
0.004
0.002
0.000
0
100
200
300
400
500
T(°C)

Fig. 13.

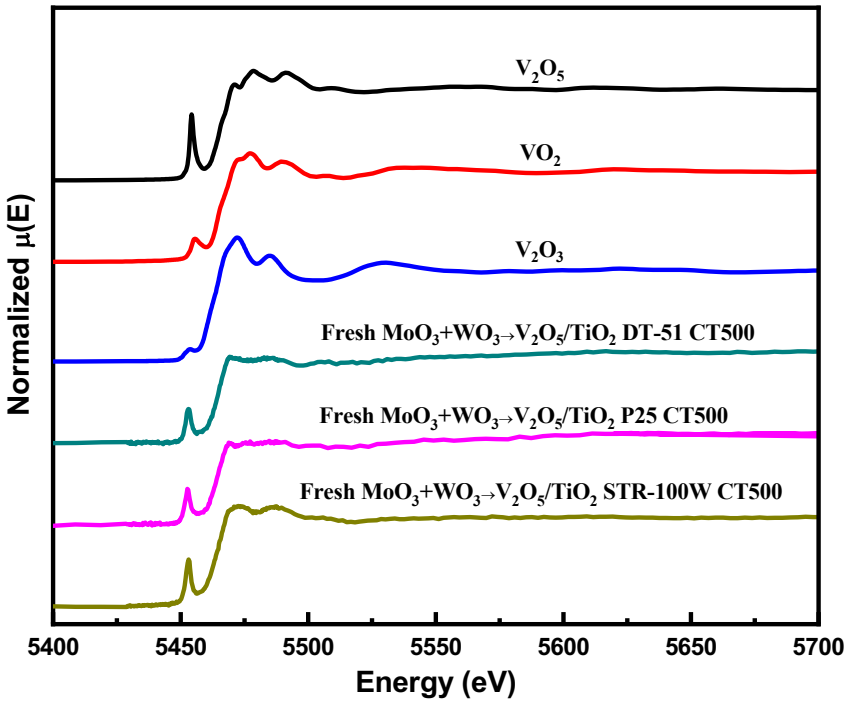
V2O5
VO2
V2O3
Fresh MoO3+WO3→V2O5/TiO2 DT-51 CT500
Fresh MoO3+WO3→V2O5/TiO2 P25 CT500
Fresh MoO3+WO3→V2O5/TiO2 STR-100W CT500
Normalized μ(E)
5400
5450
5500
5550
5600
5650
5700
Energy (eV)

Fig. 14.

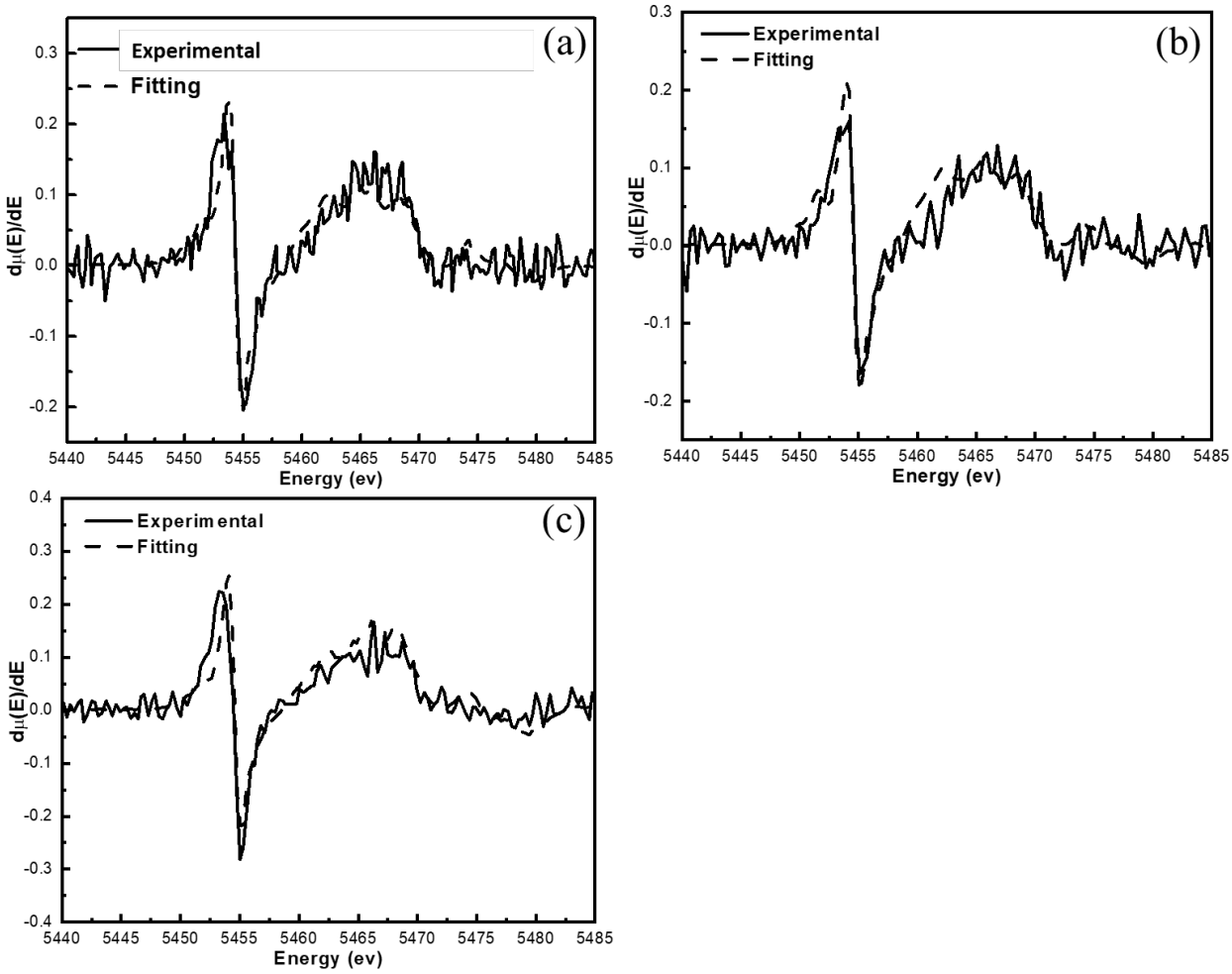

Fig. 15.

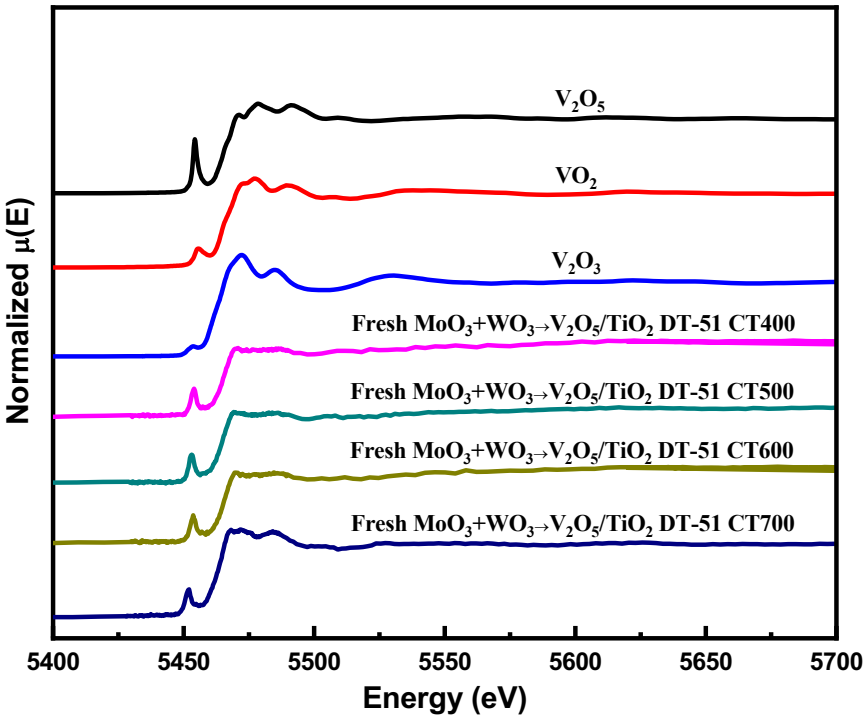
V2O5
VO2
V2O3
Fresh MoO3+WO3→V2O5/TiO2 DT-51 CT400
Fresh MoO3+WO3→V2O5/TiO2 DT-51 CT500
Fresh MoO3+WO3→V2O5/TiO2 DT-51 CT600
Fresh MoO3+WO3→V2O5/TiO2 DT-51 CT700
Normalized μ(E)
5400
5450
5500
5550
5600
5650
5700
Energy (eV)

Fig. 16.

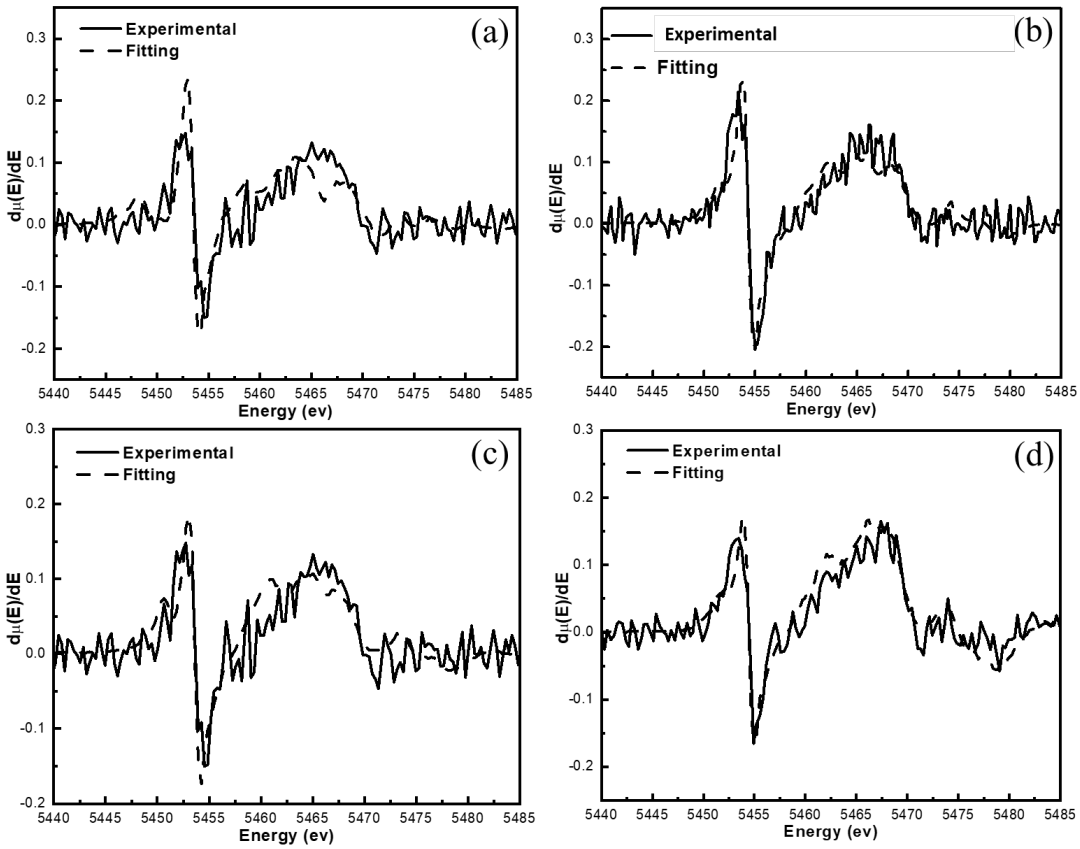
(a)
(b)
(c)
(d)
Experimental
Fitting
$d\mu(E)/dE$
Energy (ev)
0.3
0.2
0.1
0.0
-0.1
-0.2
5440
5445
5450
5455
5460
5465
5470
5475
5480
5485

Fig. 17.